Hippo pathway and Bonus control developmental cell fate decisions in the *Drosophila* eye

Heya Zhao[1], Kenneth H. Moberg[2], Alexey Veraksa[1, 3, *]

[1] Department of Biology, University of Massachusetts Boston, Boston, MA, 02125, USA
[2] Department of Cell Biology, Emory University School of Medicine, Atlanta, GA, 30322, USA
[3] Lead Contact
* Correspondence: alexey.veraksa@umb.edu

Abstract

The Hippo pathway controls organ growth, however its role in cell fate determination and the underlying mechanism is not well understood. Here, we uncover the function of the Hippo pathway in developmental cell fate decisions in the *Drosophila* eye, exerted through the interaction of Yorkie (Yki) with a transcriptional regulator Bonus (Bon). Activation of either Bon or Yki is sufficient to promote epidermal fate at the expense of eye fate through the recruitment of multiple transcriptional and post-transcriptional regulators. Transcriptome analysis reveals that Bon and Yki jointly upregulate epidermal differentiation genes and downregulate Notch target genes that modulate the eye-to-epidermal fate switch. The Hippo pathway and Bon also control the early eye-antennal specification, with activated Yki and Bon suppressing eye fate and promoting antennal fate. Our work has revealed that the Hippo pathway and Bon control cell fate decisions during *Drosophila* eye development at multiple levels.

Keywords: Yki, TIF1 family, cell fate, eye specification, Notch, E(spl)-C, HDAC1, Su(var)2-10, transcriptional regulation, protein interaction

Introduction

Organ growth and cell fate determination are critical processes in organism development. These processes are controlled and kept in balance by multiple signaling pathways whose dysregulation leads to developmental abnormalities and diseases. Such signaling pathways include the evolutionarily conserved Hippo pathway, which is implicated in various physiological functions and pathological conditions including organ growth, cell differentiation, tissue regeneration, and oncogenesis (Kulkarni et al., 2020; Zheng and Pan, 2019). The Hippo pathway transduces the upstream regulatory signals, such as cell-cell adhesion and mechanical forces, to transcriptional outputs that mediate cellular functions such as proliferation and survival (Misra and Irvine, 2018; Yu and Guan, 2013). The core Hippo pathway acts via the Hippo (Hpo)/Warts (Wts) kinase cascade to negatively regulate the activity of the transcriptional coactivator Yorkie (Yki), which associates with DNA-binding proteins such as Scalloped (Sd) to control gene expression (Zheng and Pan, 2019). The canonical transcriptional targets of the Yki-Sd complex in *Drosophila* include *cyclin E* (*cycE*), *death-associated inhibitor of apoptosis 1* (*diap1*), *bantam* microRNA (*mir-ban*), and *expanded* (*ex*); these factors promote proliferation, inhibit apoptosis, and enable negative feedback regulation (Pan, 2010). Although increasing evidence supports an essential role of the Hippo pathway in cell fate determination in multiple biological contexts (Davis and Tapon, 2019; Zheng and Pan, 2019), the cellular mechanisms remain poorly understood.

The *Drosophila* eye serves as an excellent platform to study cell fate determination due to its dispensability for viability and precisely controlled developmental patterning (Hoge, 1915; Kumar, 2018; Treisman, 2013). Most of the *Drosophila* adult head structures develop from the larval eye-antennal disc, with the compound eye and ocelli originating from the eye disc compartment, the antenna and maxillary palp from the antennal compartment, and the head epidermis from the tissues surrounding the two compartments (Dominguez and Casares, 2005). The segregation and mutual antagonism of the eye, antennal, and head epidermal fates, which begins at the second instar larval stage (L2), is regulated by several signaling pathways including Notch, EGFR, Wnt, and Hedgehog, and many eye-antennal specification genes such as *eyeless* (*ey*), *cut* (*ct*), and *homothorax* (*hth*) (Kumar, 2018; Kumar and Moses, 2001; Wang and Sun, 2012; Weasner and Kumar, 2013). Alteration of these signaling pathways and fate determination genes can cause a switch from one fate to another, leading to corresponding homeotic transformations of the affected structures (Kumar, 2018; Ordway et al., 2021). Key patterning events in the eye are linked to a wave of differentiation called the morphogenetic furrow (MF) that starts in the early third instar larval stage (L3) and proceeds from the posterior to the anterior of the eye disc, resulting in the differentiation of ommatidia, each consisting of photoreceptor cells, cone cells, pigment cells and interommatidial bristles (Treisman, 2013).

Previous studies of the role of the Hippo pathway in *Drosophila* eye differentiation focused on MF progression, terminal differentiation of photoreceptor cells, and regulation of peripodial epithelium formation (Jukam et al., 2013; Pojer et al., 2021; Wittkorn et al., 2015; Zhang et al., 2011). Studies of *ex*, *Merlin* (*Mer*) and *mob as tumor suppressor* (*mats*) mutants have suggested a possible earlier and broader impact of the Hippo pathway on eye specification

(Boedigheimer and Laughon, 1993; Lai et al., 2005; McCartney et al., 2000), however, how the Hippo pathway may control the cell fate decisions among the eye, antenna, and head epidermis remains elusive.

The transcriptional output of Yki and its mammalian orthologs YAP/TAZ primarily involves gene activation, particularly on classical Hippo targets controlling growth regulation (Meng et al., 2016; Zheng and Pan, 2019). However, other studies in mammalian systems have suggested that the YAP/TAZ-TEAD (Sd ortholog) complex can also function as a transcriptional repressor on non-canonical target genes (Beyer et al., 2013; He et al., 2020; Kim et al., 2015). Whether in other species the YAP/TAZ-TEAD complex can function as a transcriptional repressor, or as both an activator and repressor in a gene-specific manner, remains unknown.

We reasoned that the Hippo pathway may have a novel function in controlling the eye-antenna-epidermis fate determination through yet unknown interactors that regulate the transcriptional output of the Yki-Sd complex. To identity such interactors, we performed *in vitro* and *in vivo* proteomic analyses of *Drosophila* Yki and identified a novel Yki-interacting protein, Bonus (Bon). Bon is the only *Drosophila* ortholog of mammalian Transcriptional Intermediary Factor 1 (TIF1) family proteins including TIF1α (TRIM24), TIF1β (TRIM28/KAP1), TIF1γ (TRIM33), and TIF1δ (TRIM66) (Beckstead et al., 2001; Cammas et al., 2012). TIF1 family proteins associate with chromatin and regulate transcriptional activation and repression as well as protein ubiquitination, and are implicated in cancer (Cammas *et al.*, 2012; McAvera and Crawford, 2020). *Drosophila* Bon is a broadly expressed chromatin-associated protein that couples nuclear receptors and transcriptional co-regulators and can regulate heterochromatin formation for gene activation or repression in a gene-specific manner (Beckstead *et al.*, 2001; Beckstead et al., 2005; Ito et al., 2012). Bon is essential for nervous system development, metamorphosis, and cell survival (Allton et al., 2009; Beckstead *et al.*, 2001; Ito *et al.*, 2012; Salzberg et al., 1997).

Here, we present evidence for a linked function of Bon and Yki in controlling major cell fate decisions during the development of the *Drosophila* eye. Activation of Bon or Yki can induce the formation of ectopic epidermal trichomes in the eye, suggesting a cell fate switch from the eye to the epidermal fate. Through analysis of Yki interactors and Bon proteome, we have identified multiple transcriptional and post-transcriptional regulators that are necessary for this switch. Using transcriptome analysis of *Drosophila* pupal eyes, we have found that Bon and Yki jointly upregulate multiple epidermal differentiation genes and downregulate several Notch target genes that modulate trichome induction in the eye. Furthermore, we showed that the Hippo pathway and Bon can regulate the early eye-antennal specification, with activated Yki and Bon repressing the eye fate and promoting the antennal fate. Overall, we have identified a novel function of the Hippo pathway in the eye-antenna-epidermis cell fate decisions during *Drosophila* eye development. This function requires the interaction of Yki with Bon and their recruitment of coregulators, as well as their transcriptional control of a non-canonical set of target genes.

Results

Bon is a novel Yki interactor

To identify new regulators and functions of the Hippo pathway, we performed affinity purification-mass spectrometry (AP-MS) using *Drosophila* embryos expressing Yki-EGFP with a ubiquitous driver *da-GAL4* (Wodarz et al., 1995), as well as cultured *Drosophila* S2 cells expressing Yki-SBP (see Method Details). We identified the core Hippo pathway components, accessory regulators, as well as several putative novel Yki interactors, including Bon (Figure 1A, Table S1) (Kwon et al., 2013; Oh et al., 2014; Zheng and Pan, 2019). We confirmed the interaction between Bon and Yki by co-immunoprecipitation (co-IP) of tagged Bon and Yki proteins in S2 cells (Figures 1C-1D). Bon contains two adjacent PPxY motifs (PPLY^{507} and PPSY^{585}) that may direct its binding with Yki, given that other proteins with multiple PPxY motifs were shown to bind the WW domains in Yki (Figure 1B) (Badouel et al., 2009; Oh *et al.*, 2014; Zhang et al., 2015). Mutating the key tyrosine residue to alanine in either single or both WW domains in Yki strongly reduced its binding to Bon, with the first WW domain (WW1) showing a stronger reduction in binding upon mutation (Figure 1C). Similarly, substituting tyrosine with alanine in one or both PPxY motifs in Bon also largely reduced its binding to Yki, with a stronger reduction by the mutation in the second PPxY motif (PPxY2) (Figure 1D). These results indicate that Bon interacts with Yki through PPxY motifs in Bon and WW domains in Yki.

Activation of Bon or Yki causes a cell fate switch from the eye to the epidermis

We next sought to investigate whether Bon is involved in Yki-mediated tissue overgrowth in adult eyes and larval wing discs, a standard test for Hippo pathway activity. However, RNAi knockdown of Bon did not affect the overgrowth induced by Yki overexpression (Figures S1A-S1C). Loss-of-function *bon* mutants exhibit ectopic abdominal peripheral neurons in the embryo (Beckstead *et al.*, 2001; Salzberg *et al.*, 1997). However, we found that null mutants of *wts* (*wts*^{X1}) and *yki* (*yki*^{B5}) did not show loss or gain of peripheral neurons and did not affect the ectopic neuron phenotype in null (*bon*^{21B}) or hypomorphic (*bon*^{487}) *bon* mutant embryos (Figure S1D). These results suggest that Yki and Bon have independent functions in growth regulation and embryonic peripheral nervous system (PNS) development.

Interestingly, overexpression of Bon with *pGMR-GAL4*, which drives expression in all cells after the MF and persists through pupal eye development (Ellis et al., 1993; Hay et al., 1994), resulted in the formation of trichomes on the surface of adult eyes, reduction in the number of ommatidia, and disruption of the ommatidial array (Figures 2A-2B and S2A), which is consistent with a previous report (Tardi et al., 2012). Trichomes are actin-rich, non-neuronal apical extensions, which are present on insect epidermal cells but not on the retina (Arif et al., 2015; Delon et al., 2003). The trichome induction and ommatidial suppression suggest that the eye cells can be switched to an alternative epidermal fate by Bon overexpression.

To examine whether the Hippo pathway is involved in this fate switch, we overexpressed or knocked down key components of the Hippo pathway in the Bon overexpression background and quantified the trichomes. We found that Yki overexpression or hyperactivation (via *wts* knockdown) increased the number of Bon-induced trichomes (Figures 2C-2D and 2H). In contrast, knockdown of *yki* or *sd* strongly suppressed Bon-induced trichomes (Figures 2E-2F,

2H, and S2A). These results suggest that the core Hippo pathway and the transcriptional activity of Yki are essential for Bon-induced trichome formation in adult eyes. Furthermore, overexpression of Bon-PPxA, a Bon mutant with both PPxY motifs mutated to PPxA that cannot bind to Yki (see Figure 1D), resulted in significantly fewer trichomes and less disrupted ommatidia (Figures 2G-2H), indicating that the interaction with Yki is required for Bon to induce trichomes and suppress ommatidia. Together, these results suggest that the Hippo pathway regulates Bon-induced switch from the eye fate to the epidermal fate.

We then investigated whether activation of Yki alone can induce trichomes in adult eyes. Indeed, overexpression of wild-type Yki under *pGMR-GAL4* resulted in trichome formation in the eye (Figures 2I and S2B). Overexpression of constitutively active Yki-S168A, a Yki mutant insensitive to Wts phosphorylation and inhibition (Oh and Irvine, 2008), induced even more trichomes (Figures 2J, 2O, and S2C). Knockdown of *wts* also induced more trichomes than overexpression of wild-type Yki (Figures 2K, 2O, and S2D). These results suggest that Yki activation promotes trichome formation in adult eyes, with the number of trichomes correlating with Yki activity levels. Knockdown of *bon* strongly suppressed trichome formation induced by wild-type Yki, Yki-S168A, and *wts*-RNAi (Figures 2L-2N, 2P-2R, and S2B-S2F), suggesting that Bon is necessary for trichome formation induced by activated Yki.

Yki and Bon are mutually dependent for trichome initiation in the eye

Next, we investigated the timing of trichome formation in the eye, and whether Bon and Yki are mutually dependent for trichome initiation. Previous studies have suggested that the establishment of trichomes/prehairs in the pupal wing occurs at 30-36 hrs after puparium formation (APF), while trichomes on the notum initiate at 38-39 hrs APF (Chanut-Delalande et al., 2014; Delon *et al.*, 2003). We immunostained the pupal eyes for the trichome marker F-actin at different time points from 32 hrs to 44 hrs APF, and found that Bon-induced trichomes are initiated at 40 hrs APF, and are easily visible at 44 hrs APF (Figures S3A-S3F, and 3A-3F). Pupal eyes overexpressing Bon developed fewer ommatidia but had more interommatidial cells from which the trichomes derive (Figure 3B). Knockdown of *yki* strongly suppressed the initiation of Bon-induced trichomes and largely rescued the loss of ommatidia and gain of extra interommatidial cells (Figure 3C), suggesting that Yki is required for these eye defects resulting from Bon overexpression.

Similarly, we found that trichomes induced by Yki-S168A in the eye were also easily visible at the mid-pupal stage (Figure 3D). Consistent with previous reports, overexpression of Yki-S168A resulted in increased numbers of interommatidial cells and interommatidial bristles in the pupal eye, and often exhibited disrupted ommatidial array (Figure 3D) (Hamaratoglu et al., 2006; Huang et al., 2005; Nolo et al., 2006). These extra interommatidial cells generated trichomes, and some cells even had multiple trichomes per cell. Knockdown of *bon* strongly suppressed the initiation of trichomes, suggesting that Bon is necessary for the establishment of the epidermal fate in the eye resulting from Yki-S168A overexpression (Figures 3E-3F). Together, these results suggest that overactivation of either Bon or Yki alone can cause a switch from the eye to the epidermal cell fate and initiate trichome development, in a mutually dependent manner.

Svb/Ovo and Bon interactors are required for Bon- and Yki-induced trichomes in adult eyes

We further sought to investigate the mechanism of trichome formation in the eye and the factors that contribute to this process. The transcription factor Shavenbaby/Ovo (Svb/Ovo) plays a central role in the formation and patterning of epidermal trichomes (Arif *et al.*, 2015; Chanut-Delalande et al., 2006). The *svb/ovo* gene locus encodes three major protein isoforms: somatic-specific Svb, germline-specific transcriptional repressor OvoA, and germline-specific transcriptional activator OvoB (Andrews et al., 2000). Interestingly, overexpression of OvoB or Svb using *GMR-GAL4* in the eye resulted in trichome formation that is reminiscent of Bon and Yki overexpression phenotypes (Delon *et al.*, 2003). Moreover, Svb interacts with Yki and activates the Yki target gene *diap1* to protect renal stem cells from apoptosis (Bohere et al., 2018). Thus, we wondered if Svb/Ovo was involved in the regulation of Bon- and Yki-induced trichomes in adult eyes. Overexpression of OvoB enhanced Bon and Yki-S168A induced trichomes, while overexpression of OvoA, or knockdown of *svb* using an RNAi line that specifically targets somatic *svb*, strongly suppressed Bon- and Yki-S168A-induced trichomes (Figures 4A-4F, 4K, 4O and S4A-S4B), suggesting that Svb/Ovo is essential in the process of trichome formation in the eye induced by Bon or Yki overexpression.

We then asked which additional cofactors are recruited by Bon to regulate the trichome formation in the eye. To answer this question, we performed AP-MS using Bon-SBP expressed in *Drosophila* S2 cells and analyzed the Bon interactome (Figure 4G, Table S2). Yki was identified as one of the top Bon interactors, further validating their interaction (Figure 4G). In addition, we identified Histone deacetylase 1 (HDAC1), Suppressor of variegation 2-10 (Su(var)2-10), and Heterogeneous nuclear ribonucleoprotein at 27C (Hrb27C) as top Bon interactors (Figure 4G). HDAC1 is a transcriptional corepressor that acts through histone modification and is a key component of several chromatin remodeling complexes, such as NuRD, Sin3 and CoRest (Kelly and Cowley, 2013; Seto and Yoshida, 2014). Su(var)2-10 belongs to the PIAS family of SUMO ligases and controls gene transcription and *Drosophila* eye specification (Betz et al., 2001; Hari et al., 2001; Ninova et al., 2020a; Ninova et al., 2020b). Hrb27C is an abundant *Drosophila* hnRNP that is involved in various aspects of post-transcriptional mRNA regulation and is implicated in the modulation of Yki activity (Goodrich et al., 2004; Mach et al., 2018). We tested whether these three Bon interactors are involved in the formation of Bon- and Yki-induced trichomes in adult eyes. Knockdown or overexpression of *HDAC1* strongly suppressed or enhanced, respectively, both Bon- and Yki-S168A-induced trichomes (Figure 4H, 4K, 4L, 4O, and S4A-S4B), and knockdown of *Su(var)2-10* or *Hrb27C* suppressed these trichomes (Figure 4I-4K, 4M-4O, and S4A-S4B). These results suggest that the Bon interactors HDAC1, Su(var)2-10, and Hrb27C are all necessary for the induction of the epidermal fate in the eye by either Bon or Yki.

Bon and Yki control the eye-to-epidermis fate switch through transcriptional regulation of joint target genes

Since Bon, Yki and their interactors that contribute to trichome formation in the eye are all transcriptional or post-transcriptional regulators, we hypothesized that the cell fate switch

induced by Bon and Yki in the eye is mediated by a unique set of transcriptional targets. To identify target genes that are jointly controlled by Bon and Yki, we performed RNA sequencing (RNA-seq) using 40-41 hr APF pupal eyes (when the trichomes initiate) that overexpressed Bon, with and without a simultaneous knockdown of *yki* by RNAi. Through differential gene expression analysis, we identified 216 genes as Yki-dependent Bon-activated genes, and 119 genes as Yki-dependent Bon-repressed genes (Figures 5A, S5A-S5B, and Table S3). Correlation coefficient analysis revealed the significantly concordant regulation of gene expression, suggesting that Bon and Yki work together in gene regulation (Figure 5B), which is consistent with the genetic results on trichome formation. Also, *ex* and *Rhodopsin 5* (*Rh5)*, which are known target genes of Yki, were upregulated by Bon overexpression and downregulated by *yki* RNAi (Figures 5A and S5A-S5B). These results suggest that Bon and Yki function together to regulate gene transcription in pupal eyes.

We then evaluated the genes that were jointly regulated by Bon and Yki by Gene Ontology analysis of Biological Process (GO_BP, Table S4). Yki-dependent Bon-activated genes were enriched for GO terms “epidermal cell differentiation” and “cuticle development”, while Yki-dependent Bon-repressed genes were enriched for GO terms “compound eye development” and “Notch signaling pathway”, consistent with the genetic function of Bon and Yki in promoting epidermal trichomes and suppressing eye differentiation (Figure 5C). The Yki-dependent Bon-activated epidermal genes, *shavenoid* (*sha*), *forked* (*f*), *nyobe* (*nyo*), and *neyo* (*neo*), are known target genes of Svb that are essential for the formation and patterning of trichomes in epidermis, suggesting that they may mediate Bon- and Yki-induced trichome formation in the eye (Figure 5A and 5C) (Arif *et al.*, 2015). The Yki-dependent Bon-repressed Notch pathway genes, *E(spl)mdelta-HLH*, *E(spl)m3-HLH* and *E(spl)m2-BFM*, are members of the Enhancer of split gene complex (E(spl)-C) which is a major transcriptional target of Notch (Figure 5A and 5C) (Knust et al., 1992; Lai et al., 2000). Two other Notch target genes, *ct* and *Transcription factor AP-2* (*TfAP-2*), were also identified among Yki-dependent Bon-repressed genes (Figure 5A) (Kerber et al., 2001; Micchelli et al., 1997). Notch, E(spl)-C, Ct and TfAP-2 are critical for cell fate establishment in the *Drosophila* eye, suggesting that downregulation of Notch targets by Yki and Bon may mediate the suppression of eye differentiation (Cagan and Ready, 1989; Kumar and Moses, 2001; Lai and Rubin, 2001; Monge et al., 2001; Wang and Sun, 2012).

We validated the transcriptional regulation of *sha*, *f*, *E(spl)m3-HLH*, *E(spl)m2-BFM*, and *E(spl)mdelta-HLH* by Bon and Yki using target-specific qRT-PCR, which generally confirmed the RNA-seq findings (Figure 5D). An incomplete rescue of *sha*, *E(spl)m2-BFM* and *E(spl)m3-HLH* expression by *yki* knockdown is likely due to a partial reduction of *yki* by RNAi (Figure 5D and Table S3). We then investigated whether these joint target genes of Bon and Yki mediate trichome formation. Overexpression of Sha enhanced, whereas knockdown of *f* suppressed, the Bon- and Yki-S168A-induced trichomes in the eye (Figures 5E-G, 5J, 5K-M, 5P, and S5C-S5H). This suggests that *sha* and *f* promote Bon- and Yki-induced trichome formation in the eye, consistent with their activation by Bon and Yki. In contrast, overexpression of E(spl)mdelta-HLH and E(spl)m3-HLH suppressed the trichomes induced by Bon and Yki-S168A, consistent with their repression by Bon and Yki (Figures 5H-5J and 5N-5P). Together, these results suggest

that Bon and Yki promote epidermal fate in the eye through joint activation of *sha* and *f*, and the repression of *E(spl)-C* genes.

Yki and Bon suppress eye fate and promote antennal fate

Previous work showed that the Notch signaling pathway promotes the eye fate and suppresses the antennal fate (Kumar and Moses, 2001; Kurata et al., 2000; Monge *et al.*, 2001). We found that Bon and Yki repress several Notch target genes, and also upregulate an antenna-specific odorant receptor gene *Or47b*, as well as a group of gustatory receptor genes *Gr64a-f* which are expressed in multiple sensory organs including the antenna but excluding the eye (Figures 5A, 5C, and S5A-S5B) (Barish et al., 2017; Fujii et al., 2015; Menuz et al., 2014; Vosshall, 2001). This raised an intriguing possibility that gain of function of Bon and Yki may result in an eye-to-antenna transformation. To explore this hypothesis, we used the *ey-GAL4* driver whose expression is restricted to the eye disc from the L2 stage, and followed Hth and Ct as antennal markers, and Elav as the differentiated neuron/eye marker (Blochlinger et al., 1993; Kumar and Moses, 2001; Pai et al., 1998; Wang and Sun, 2012). Knockdown of *wts* or overexpression of Yki-S168A with two independent lines under *ey-GAL4* significantly suppressed the eye field in most cases, with respective penetrance of 56% (*wts*-RNAi), 77% (*yki-S168A*-1) and 85% (*yki-S168A*-2), and even occasionally led to a complete eye-to-antenna transformation, with respective penetrance of 11%, 7% and 6% (Figures 6A-6C, 6M, S6A-S6B, S6E-S6G, and Table S5). Remarkably, *wts* knockdown or Yki-S168A overexpression led to a clear eye-to-antenna transformation in some adult flies (Figures 6E-6G). Overexpression of wild-type Yki under *ey-GAL4* resulted in a suppression of the eye field, but without eye-to-antenna transformation (Figures S6H-H'''). Together, these results show that early hyperactivation of Yki across the eye field can switch the fate of the eye towards that of an antenna.

Next, we asked if Bon contributes to Yki-S168A-induced eye-to-antenna transformation. In eye-antennal discs, *bon* knockdown significantly rescued the loss of eye field (from 77% to 3%, and 85% to 43%, with two independent lines), and suppressed the formation of double antennae (from 7% to 0%, and 6% to 2.5%, with two lines) due to Yki-S168A overexpression (Figures 6D, 6M, S6C-S6D, and Table S5). In adults, *bon* knockdown also largely restored the normal eye field (Figure 6H). We then asked if *E(spl)-C* or HDAC1 were involved in Yki-S168A-induced eye-to-antenna transformation. Overexpression of E(spl)m3-HLH or knockdown of *HDAC1* significantly rescued the loss of eye field, and E(spl)m3-HLH also completely suppressed the formation of double antennae (Figures 6I-6M and Table S5). Together, these results suggest that similar to their roles in the late eye-to-epidermis cell fate change, Bon, HDAC1 and E(spl)m3-HLH also modulate the early eye-to-antenna transformation induced by hyperactivated Yki.

We then investigated the effect of Bon itself in eye-antennal specification. Overexpression of Bon under *ey-GAL4* led to a suppression of the differentiated eye field with a penetrance of 20% (Figures 6N and S6I). In adults, Bon overexpression resulted in a complete or partial loss of the eye with a penetrance of 18%, and often exhibited protrusion of an antenna-like outgrowth (Figure 6O). This was in contrast with the normal eye field formed in Bon-PPxA overexpression (Figures S6J, Table S5). As an alternative to *ey-GAL4*, we also used a more localized driver *bi-*

GAL4, which drives expression in the dorsal and ventral margins of the eye disc (Tare et al., 2013). Yki overexpression under *bi-GAL4* can result in a suppression of Elav expression (Wittkorn *et al.*, 2015). We found that overexpression of Bon under *bi-GAL4* also suppressed Elav at the margins, whereas overexpression of Bon-PPxA did not (Figures S6K-S6M and S6P). Knockdown of Bon interactors *Su(var)2-10* or *HDAC1* significantly rescued the loss of Elav expression (Figures S6N-S6P). These results suggest that Bon can suppress the eye fate and may promote the antennal fate, and that this effect requires interaction with Yki and the participation of Bon-interacting proteins.

To determine whether the eye-antennal specification is under the control of endogenous *yki* and *bon*, we tested the effects of their loss in the antenna using the *hth-GAL4* driver. Since the eye and antennal fates are mutually antagonistic and reciprocally transformable (Wang and Sun, 2012), we hypothesized that the loss of *yki* and/or *bon* in the antenna would result in a switch towards the eye fate. Indeed, knockdown of *yki* alone resulted in a variable degree of antenna loss with 100% penetrance, and a moderate antenna-to-eye transformation (13% penetrance) (Figures 7A-7B, 7D, S6Q-S6T, and Table S5). This antenna-to-eye transformation exhibited partial loss of Ct and gain of Elav in the antennal field, suggesting a suppression of the antennal fate and differentiation of an ectopic eye (Figure 7B). Strikingly, a double knockdown of *yki* and *bon* resulted in a severe antenna-to-eye transformation (26% penetrance), in which the antennal field marked by Ct was restricted to the center of the eye-antennal disc, and the ectopic Elav pattern resembled a mirror-image duplication of the endogenous eye field (Figures 7C-7D). These results demonstrate that endogenous Yki and Bon are necessary for the specification of the antennal fate and the suppression of the eye fate.

Discussion

Our results have revealed a previously unappreciated and profound role of the Hippo pathway in controlling cell fate determination in the *Drosophila* eye (Figure 7E-7G). This function depends on the activity of the novel Yki interactor, Bon. We have uncovered a joint regulatory program in which Yki and Bon interact, and likely act as a module that is a part of larger multiprotein complexes. Rather than controlling growth or PNS differentiation, which represent independent functions of Yki and Bon (Figure 7E), the Yki-Bon module regulates the proper segregation of eye, antennal, and epidermal fates in the developing eye. This regulation occurs at multiple levels, involving the promotion of the antennal and epidermal fates, and the suppression of the eye fate (Figure 7F). Yki and Bon thus contribute to the mutual antagonism among the different cell fates, which is necessary for the correct overall patterning of the eye and other head structures.

The involvement of Yki and Bon at different levels in the eye patterning hierarchy is demonstrated by two lines of evidence. First, we found that the timing and extent of Yki and Bon genetic manipulations determine the overall final phenotypes observed (Figure 7G). Thus, an early and widespread overexpression of Yki-S168A or knockdown of *wts* with *ey-GAL4* before the eye-antennal segregation can result in a complete suppression of the eye field and duplication of the antenna. In contrast, using wild type Yki with the same driver, or using *pGMR-*

GAL4 or *bi-GAL4* that are expressed later and in a more restricted pattern, leads to milder phenotypes such as the formation of ectopic epidermal trichomes in the adult eye. Likewise, an early and widespread knockdown of both *bon* and *yki* in the antenna using *hth-GAL4* results in the loss of antennal structures and a severe expansion of the eye field into the antennal field. Second, our RNA-seq analysis identified multiple genes under the joint control of Bon and Yki that are not canonical Hippo pathway targets (Figure 7F). Positively regulated genes include *sha*, *f*, *nyo* and *neo*, all involved in trichome differentiation and thus establishment of the epidermal fate. In addition, we found that Yki and Bon upregulate antennal markers *Gr64a-f* and *Or47b*. In contrast, Yki and Bon repress Notch targets *E(spl)-C*, *ct*, and *TfAP-2* that are essential for the eye fate. Collectively, these data suggest that Yki and Bon jointly control both the early segregation between the eye and the antennal fields, and the later process of epidermal differentiation (Figure 7G).

Our data uncovered an unexpected layer of control over eye specification exerted by Yki and Bon at the level of Notch target genes. Notch signaling is required and sufficient for the promotion of the eye fate and suppression of the antennal fate during early eye-antennal specification, and is required for successful differentiation and patterning of the ommatidia (Cagan and Ready, 1989; Kumar and Moses, 2001; Kurata *et al.*, 2000; Monge *et al.*, 2001). Although we have identified several Notch targets that are repressed by Bon and Yki, Notch itself and the key Notch pathway components, Serrate, Delta, and Su(H), were not transcriptionally regulated, and were not found in Yki or Bon protein interactomes (Tables S1-S3). Therefore, we propose that Bon and Yki repress Notch targets such as *E(spl)-C* genes independently from upstream Notch signaling, and thus contribute to the suppression of eye fate and promotion of alternative fates. We note that not all *E(spl)-C* genes are under Bon and Yki control, implying context-dependent regulation and functional divergence of *E(spl)-C* genes, as suggested by previous studies (Table S3) (Couturier et al., 2019; Ligoxygakis et al., 1999).

We have shown that Svb/Ovo is required for the formation of ectopic trichomes in the eye that are induced by Yki and Bon. Though Svb/Ovo itself was not regulated, we found that its direct targets *sha*, *f*, *neo* and *nyo* were all transcriptionally activated by Bon and Yki (Table S3). The Svb/Ovo protein interacts with Yki (Bohere *et al.*, 2018), and thus may contribute to Yki- and Bon-mediated control of these target genes. Svb/Ovo and its targets are required for the formation and patterning of trichomes on normal epidermis, thus we also studied the effects of Yki and Bon in adult wings. We found that overexpression of wild type but not PPxA mutant of Bon increased the number of trichomes, whereas a simultaneous knockdown of *yki* and *bon* reduced trichome density (perhaps in part as an indirect consequence of potential modulation of cell size) and disrupted trichome morphology in the wing (Figure S7). These results indicate that Yki and Bon may also regulate differentiation in the normal epidermis, as suggested by previous studies (Fang and Adler, 2010; He et al., 2005). Analysis of the published RNA-seq data in *wts* mutant wing discs revealed upregulation of *f* and *nyo* (Table S6) (Oh et al., 2013), raising a possibility that Yki and Bon may control epidermal differentiation in the wing via joint regulation of epidermal specification genes.

To determine whether the transcriptional targets of Yki and Bon are under their direct control, we analyzed the published ChIP-seq datasets for Yki and Bon, and the DamID-seq dataset for Sd (Negre et al., 2011; Oh *et al.*, 2013; Vissers et al., 2018). This analysis revealed that Yki, Sd and Bon all bind to the *E(spl)-C* gene locus, suggesting that *E(spl)mdelta-HLH*, *E(spl)m3-HLH* and *E(spl)m2-BFM* are potential direct targets of these proteins (Figure S5I-J, Table S6). Yki and Sd also bind to *ct* and *TfAP-2*, suggesting that these Notch target genes are also under their direct control (Table S6). The absence of Bon peaks on the *ct* and *TfAP-2* genes is likely due to the low number of total peaks detected in Bon ChIP-seq (Table S6). Yki, Sd and Bon did not associate with the epidermal differentiation genes and antennal sensory receptor genes, except for Yki binding to *neo*, suggesting that the activation of these genes by Bon and Yki may be indirect (Table S6). Interestingly, ChIP-seq of Svb also showed its association with *ct* and *E(spl)-C* genes (Figure S5I, Table S6) (Menoret et al., 2013), raising a possibility that Svb may also regulate eye fate determination together with Yki and Bon through transcriptional regulation of Notch target genes.

Through the analysis of the Bon protein interactome, we uncovered and functionally validated several transcriptional cofactors, including epigenetic regulators, that participate in the joint regulation by Bon and Yki. Histone deacetylase HDAC1 has been implicated in the negative regulation of several signaling pathways including Notch (Borggrefe and Oswald, 2009), and it is likely that Bon and Yki recruit HDAC1 to repress Notch target genes. This function may involve another corepressor, CoRest, that was also identified as a Bon interactor (Figure 4). The involvement of epigenetic regulators in transcriptional regulation by Bon and Yki is further exemplified by the Bon interactor Su(var)2-10, which has a role in chromatin SUMOylation and piRNA target gene silencing (Ninova *et al.*, 2020a; Ninova *et al.*, 2020b). Finally, though Hrb27C is an hnRNP with a known role in Yki regulation in the cytoplasm (Mach *et al.*, 2018), its association with Bon, a nuclear protein, suggests a possible function in the nucleus, such as the regulation of alternative splicing, degradation, or nucleocytoplasmic transport of mRNAs encoded by Bon and Yki target genes. Hrb27C may thus be involved in both cell fate determination and growth regulation mediated by the Hippo pathway, perhaps through different mechanisms in different cellular compartments.

The Hippo pathway and Bon are conserved in higher eukaryotes, and their orthologs are implicated in similar developmental contexts and diseases (Cammas *et al.*, 2012; Hergovich and Hemmings, 2012), raising a possibility of their joint control over cell fate decisions in other organisms and tissue contexts. For example, TIF1γ is required for hematopoiesis in vertebrates, and the Hippo pathway is essential for proper differentiation and proliferation of *Drosophila* blood cells (Milton et al., 2014; Rossmann et al., 2021). In addition, both the YAP/TAZ-TEAD complex and TIF1β can recruit the transcriptional corepressor NuRD complex for gene repression (Beyer *et al.*, 2013; He *et al.*, 2020; Kim *et al.*, 2015; Schultz et al., 2001). Moreover, independent transcriptome analyses of mammalian YAP/TAZ and TIF1γ revealed the potential repression and association with Notch target genes (He *et al.*, 2020; Isbel et al., 2015; Kim *et al.*, 2015; Zhao et al., 2008). This emerging evidence suggests that the cell fate determination controlled by the Hippo pathway and Bon and the underlying molecular mechanism reported

here is likely a general property of these critical transcriptional regulators in *Drosophila* and vertebrates.

Acknowledgments
We thank Spyros Artavanis-Tsakonas, Hugo J. Bellen, Claude Desplan, Jin Jiang, Eric C. Lai, Duojia Pan, Alexei Tulin, BDSC, VDRC, DGRC and DSHB for fly stocks and reagents. We thank Georg Halder, Kieran Harvey, Y Tony Ip, Kenneth Irvine, Nicolas Tapon, Barry Thompson, Can Zhang and Lei Zhang for helpful discussions. We thank Alexander Letizia and Katerina Heath for helping with plasmid constructions. This work was funded by NIH grants GM105813 and GM123136 to K.H.M. and A.V.

Author contributions
Conceptualization, H.Z., K.H.M., and A.V.; Methodology, H.Z., K.H.M., and A.V.; Formal analysis, H.Z.; Investigation, H.Z.; Resources, K.H.M. and A.V.; Data Curation, H.Z.; Writing – Original Draft, H.Z.; Writing – Review & Editing, H.Z., K.H.M., and A.V.; Visualization, H.Z.; Supervision, A.V.; Funding Acquisition, K.H.M. and A.V.

Declaration of interests
The authors declare no competing interests.

Figure Legends

Figure 1. Identification of Bonus as a Yorkie interactor
(A) The Yki protein interaction network. AP-MS results of Yki-SBP from *Drosophila* S2 cells and Yki-EGFP from embryos were analyzed with Significance Analysis of INTeractome (SAINT) (Choi et al., 2011). All the interactors (nodes) in this network were identified as significant (SAINT score ≥ 0.8). The interactions (edges) were incorporated from the STRING database and FlyBase (Szklarczyk et al., 2019; Thurmond et al., 2019).
(B) Schematic diagram showing the major domains and motifs in Yki and Bon. Note two WW domains in Yki and two PPxY motifs in Bon.
(C) Co-IP of Bon-V5 and wild-type or mutant Yki-HA expressed in S2 cells.
(D) Co-IP of Yki-HA and wild-type or mutant Bon-V5 expressed in S2 cells.

Figure 2. Activation of Bon or Yki causes a cell fate switch from the eye to the epidermis
(A-G, I-N) SEM images of adult *Drosophila* eyes expressing indicated *UAS* transgenes with the *pGMR-GAL4* driver. Crosses with Bon were carried out at 25°C, and crosses with Yki, Yki-S168A and *wts*-RNAi were set up at 25°C and shifted to 29°C after the emergence of first instar larvae. Arrowheads: interommatidial bristles, arrows: trichomes. Scale bars in left panels: 100 μm; right panels: 10 μm.
(H, O-R) Quantification of the number of trichomes in A-G (H) and I-N (O-R). *w*-RNAi-1, *w*-RNAi-2, and *GFP* were coexpressed for transgene dosage compensation. Additional images for the quantified genotypes are shown in Figure S2. Trichome numbers here and in the other figures were obtained for a 1306 μm^2 area. The number of trichomes and the number of images

quantified (n ≥ 3) for each genotype are provided in Table S5. Statistical analyses are described in Method Details.

Figure 3. Yki and Bon are mutually dependent for trichome initiation in the eye

(A-F) Pupal eyes expressing the indicated transgenes with *pGMR-GAL4* were immunostained with phalloidin (F-actin) and anti-disc large antibody (Dlg) (cell boundaries). (A-C) were at 44 hrs APF grown at 25°C, (D-F) were at 39 hrs APF grown at 29°C (equivalent to 47 hrs APF at 25°C). Arrowheads: interommatidial bristles and sockets, arrows: trichomes and the corresponding cells. Scale bars: 10 µm.

Figure 4. Svb/Ovo and Bon interactors are required for Bon- and Yki-induced trichomes in adult eyes

(A-F, H-J, L-N) SEM images of adult eyes expressing indicated *UAS* transgenes with the *pGMR-GAL4* driver. Scales bars in left panels: 100 µm; right panels: 10 µm.

(G) The Bon protein interaction network generated from AP-MS data for Bon-SBP in S2 cells showing significant interactions (SAINT score ≥ 0.8). Interactors highlighted with color were tested in genetic experiments.

(K, O) Quantification of trichome numbers for the indicated genotypes. Additional images for the quantified genotypes are shown in Figure S4.

Figure 5. Bon and Yki control the eye-to-epidermis fate switch through transcriptional regulation of joint target genes

(A) Differential gene expression analysis of RNA-seq data. Output from DEseq2 (Love et al., 2014) was plotted using $\log_2$ fold changes (FC) for *pGMR>bon-mCherry; yki*-RNAi-1 vs. *pGMR>bon-mCherry* (y axis) and that for *pGMR>bon-mCherry* vs. *pGMR>mCherry* (WT) (x axis). Dashed lines: $\log_2$ FC = ± $\log_2$ (1.5). Red circles: Yki-dependent Bon-activated genes ($\log_2$ FC ≥ $\log_2$ (1.5) on x; $\log_2$ FC ≤ -$\log_2$ (1.5) on y). Blue circles: Yki-dependent Bon-repressed genes ($\log_2$ FC ≤ -$\log_2$ (1.5) on x; $\log_2$ FC ≥ $\log_2$ (1.5) on y). All colored circles fulfill p adj. ≤ 0.05. Solid circles with labels: genes of interest. Labels underlined: genes validated with qRT-PCR.

(B) Pearson correlation coefficient analysis of genes jointly regulated by Bon and Yki. Axes are the same as in (A). All genes with absolute $\log_2$ FC ≥ $\log_2$ (1.5) and p adj. ≤ 0.05 were included in the analysis.

(C) Terms of interest from GO_BP analysis of Yki-dependent Bon-activated (red) and -repressed (blue) genes. Complete GO_BP analysis is provided in Table S4.

(D) qRT-PCR validation of the genes of interest. The genotypes were *pGMR>mCherry* (WT), *pGMR>bon-mCherry*, and *pGMR>bon-mCherry; yki*-RNAi-1.

(E-P) Regulation of Bon-induced (E-J) and Yki-S168A-induced (K-P) trichomes by the joint target genes. (E-I, K-O) SEM images of adult eyes expressing indicated *UAS* transgenes with the *pGMR-GAL4* driver. Scale bars in left panels, 100 µm; right panels, 10 µm. (J, P) Quantification of trichome numbers. Additional images for the quantified genotypes are shown in Figure S5.

Figure 6. Yki and Bon suppress the eye fate and promote the antennal fate

(A-L') L3 eye-antennal discs expressing indicated transgenes with the eye driver *ey-GAL4-1* were immunostained with anti-Hth antibody (antennal compartment, A-D) or anti-Ct and anti-Elav antibodies (antennal compartment and differentiated eye tissue, respectively, I-L). Driver expression domain was visualized by GFP (A and I). (A'-L') Schematic illustrations of the structure of the eye-antennal disc and the patterns of Hth, Ct and Elav staining in (A-L). Arrows: eye discs, arrowheads: antennal discs. Scale bars: 50 µm.
(E-H) Representative SEM images of adult heads expressing the indicated transgenes with *ey-GAL4-1*. *wts*-RNAi resulted in double antennae with triple aristae and fused a1 and a2 segments (F). Yki-S168A resulted in double or triple antennae with one arista each and an ectopic maxillary palp (G). White arrows: eyes, white arrowheads: antennal a3 segments, yellow arrowheads: aristae, white mp and yellow mp: original and ectopic maxillary palps, respectively. Scale bars: 50 µm.
(M) Quantification of the eye-antennal disc phenotypes shown in (A-L and Figures S6A-S6G). P values were determined using Fisher's exact test between normal and abnormal eye disc populations within indicated comparisons. Detailed numbers are provided in Table S5.
(N-N') L3 eye-antennal disc expressing *bon-mCherry* with *ey-GAL4-2* were immunostained with anti-Ct and anti-Elav antibodies. GFP control with the same driver and staining is shown in Figure S6I. Quantification is provided in Table S5. (N') Schematic illustration of the structure and staining in (N). Scale bars: 50 µm.
(O) Representative SEM images of adult head expressing *bon-mCherry* with *ey-GAL4-1*. White arrowhead: antennal a3 segment, yellow arrowhead: arista, yellow text: antenna-like outgrowth (al). Related *bon-PPxA-mCherry* phenotype under the same driver is shown in Figure S6J. Quantifications are provided in Table S5. Scale bars: 50 µm.

Figure 7. Joint function of Yki and Bon in *Drosophila* eye specification.
(A-C') L3 eye-antennal discs with the indicated transgenes driven by *hth-GAL4* were immunostained with anti-Ct and anti-Elav antibodies. The expression domain of the driver was visualized by GFP (A). Representative moderate antenna-to-eye transformation (B); representative severe antenna-to-eye transformation (C). (A'-C') Schematic illustrations of the structure and staining in (A-C). Scale bars: 50 µm.
(D) Quantification of the eye-antennal disc phenotypes shown in (A-C and Figures S6R-S6T). P values were determined using Fisher's exact test between normal and abnormal antennal disc populations (*GFP* vs. *yki*-RNAi-1) or severe vs. non-severe antenna-to-eye transformation (*yki*-RNAi-1*; bon*-RNAi-1 vs*. yki*-RNAi-1). Detailed numbers are provided in Table S5.
(E) Independent functions of Yki and Bon in growth regulation and embryonic PNS development, respectively.
(F) Yki and Bon jointly regulate eye specification through recruitment of transcriptional and post-transcriptional regulators and transcriptional control of a set of non-canonical target genes.
(G) The Yki-Bon complex regulates eye specification at multiple levels and at different time points in *Drosophila* development. During the early eye-antennal fate segregation, the Yki-Bon complex promotes antennal fate and suppresses eye fate. Genetic perturbations during this time result in eye/antenna mutual transformations. After the successful segregation of the eye-antennal fate and the onset of MF progression, the Yki-Bon complex promotes epidermal fate

and suppresses eye fate. Hyperactivation of Yki and Bon results in the formation of epidermal trichomes at the expense of normal ommatidia. See Discussion for further details.

Methods

Plasmid construction

pMK33-yki-SBP was generated by cloning Yki-RG isoform from pMT-yki-V5 (Zhang *et al.*, 2015) into pMK33-SBP-C vector (Yang and Veraksa, 2017). pUASTattB-yki-EGFP was generated by cloning Yki-RG and EGFP tag into pUASTattB vector (Bischof et al., 2007). pMT-yki-HA was generated by cloning Yki-RG and HA tag into pMT-V5-His vector (Invitrogen, Cat# V412020). The Y281A, Y350A mutations of WW domains in Yki were generated by Q5 Site-Directed Mutagenesis Kit (NEB, Cat# E0554S) using pMT-yki-HA as a template. The numbering of the key tyrosine residues used in this work corresponds with the first reported yki sequence (yki-RH) which has a stretch of additional 23 aa at the N-terminus (Huang *et al.*, 2005).

pMT-bon-V5, pMK33-bon-SBP and pUASTattB-bon-mCherry were generated by cloning Bon-RB isoform from pFlc-1-bon (DGRC, RE48191). The Y507A, Y585A mutations in PPxY motifs of Bon were generated by the Q5 Site-Directed Mutagenesis Kit. pUASTattB-bon-mCherry and pUASTattB-bon-Y507A Y585A-mCherry were constructed using NEBuilder HiFi DNA Assembly Cloning Kit (NEB, Cat# E5520S). All tags were added to the C-terminus of the corresponding genes.

Stable cell lines

S2 cells were transfected with pMK33-yki-SBP and pMK33-bon-SBP constructs using the Effectene transfection reagent (Qiagen, Cat# 301427). Stable cell lines were selected with medium containing 300 µg/ml of Hygromycin B (Sigma-Aldrich, Cat# H3274). Yki-SBP and Bon-SBP stable cells were induced overnight with 0.07 mM $CuSO_4$, and protein expression was verified by a western blot using anti-SBP antibody (1:1000, Santa Cruz, Cat# sc-101595).

Transgenic fly lines

pUASTattB-yki-EGFP plasmid was injected into the attP2 site in *D. melanogaster* embryos (Genetic Services, Inc). pUASTattB-bon-mCherry and pUASTattB-bon-Y507A Y585A-mCherry plasmids were injected into the attP40 site in *D. melanogaster* embryos (Rainbow Transgenic Flies, Inc). *yw*, Chr. 2 and Chr. 3 balancer stocks were used in standard crossing schemes to establish the homozygous transgenic lines.

Genetic crosses

To score the trichome phenotype, *UAS-bon-mCherry*, *UAS-yki-EGFP*, *UAS-yki-S168A-1* (*UAS-yki.S168A.GFP.HA*, BDSC: 28816) and *UAS-wts-RNAi* (VDRC: 111002) were combined with the eye driver *pGMR-GAL4* to generate *UAS-bon-mCherry/CyO wg-lacZ; pGMR-GAL4/TM6B*, *pGMR-GAL4 UAS-yki-EGFP/TM6B*, *pGMR-GAL4 UAS-yki-S168A-GFP-1/TM6B* and UAS-wts-RNAi/CyO wg-lacZ; pGMR-GAL4/TM6B fly lines, respectively. *w-RNAi-1*, *w-RNAi-2*, and *GFP* were coexpressed for transgene dosage compensation. If not indicated, overexpression of

regulators was compared to *UAS-GFP*, while knockdowns of regulators were compared to both *UAS-w-RNAi* lines and larger p values were presented.

To achieve higher GAL4 activity, all crosses with *pGMR-GAL4 UAS-yki-EGFP/TM6B* and *pGMR-GAL4 UAS-yki-S168A-GFP-1* were set up at 25°C and shifted to 29°C after 1st instar larval stage. The crosses with *UAS-wts-RNAi/CyO wg-lacZ; pGMR-GAL4/TM6B* were either set up at 25°C and shifted to 29°C after 1st instar larval stage (Figure 2) or carried out at 25°C (Figures S2E-F). All the crosses with *UAS-bon-mCherry/CyO wg-lacZ; pGMR-GAL4/TM6B* were carried out at 25°C.

All the crosses using *ey-GAL4* were carried out at 29°C except for the cross of *ey-GAL4-1* and *UAS-wts-RNAi* which was carried out at 25°C.

The cross of *da-GAL4* and *UAS-yki-EGFP* for embryo collection and affinity purification was carried out at RT.

All other crosses were carried out at 25°C.

Affinity Purification

Affinity purification from S2 cells. Blank S2 cells (control) and stable cell lines with 50 ml dense culture were induced overnight (~16 hrs) with 0.07 mM $CuSO_4$ at 25°C. Cells were collected and lysed on ice for 20 min using 1 ml of ice-cold Default Lysis Buffer (DLB) (50 mM Tris pH 7.5, 125 mM NaCl, 5% (v/v) glycerol, 0.2% (v/v) IGEPAL, 1.5 mM $MgCl_2$, 25 mM NaF, 1 mM Na_3VO_4, 1 mM DTT, and 2x cOmplete Protease Inhibitor (Roche, Cat# 11836145001, 1 tablet per 25 ml lysis buffer)). The lysate was centrifugated at 16,000 rcf for 20 min at 4°C, and the supernatant was incubated with 50 µl of packed Streptavidin beads (Thermo Fisher Scientific, Cat# 53117) for 2 hrs at 4°C with rotation. The beads were then washed 5 times with 1 ml DLB. Proteins on the beads were eluted with 300 µl DLB containing 2 mM biotin and precipitated by adding 1/10 volume of 8.74 M Trichloroacetic acid solution (TCA, Fisher Scientific, Cat# BP555-500). Precipitated proteins were washed once with 500 µl of 0.874 M TCA and four times with ice-cold acetone. The protein pellet was dried overnight at RT and incubated in 40 µl of 2x SDS sample buffer at 95°C for 5 min. Samples were assessed by silver staining using NuPAGE 4-12% Bis-Tris Protein Gel (Thermo Fisher Scientific, Cat# NP0335) and SilverQuest Silver Staining Kit (Thermo Fisher Scientific, Cat# LC6070). The protein samples for mass spectrometry were separated on a short SDS-PAGE gel (8% Tris-Glycine) followed by Coomassie blue staining. Two gel pieces (>75 kDa and < 75 kDa) for each sample were submitted to Taplin Mass Spectrometry Facility at Harvard Medical School for mass spectrometry analysis, as described (Yang and Veraksa, 2017).

Affinity purification from embryos. 5 L fly cages with apple juice plates (Yang et al., 2017) were set up for *yw* (control) and the cross *da-GAL4* x *UAS-yki-EGFP*. Flies were allowed to lay eggs for 15 hrs at RT, then the apple juice plates containing the embryos were incubated for 3 hrs at 25°C. Approximately 1 g embryos were dechorionated with 50% (v/v) Clorox bleach and washed with water. Collected embryos were then mixed with 6 ml of ice-cold DLB containing 0.5%

(v/v) IGEPAL and 10 μM MG132 in a glass homogenizer and lysed on ice using 20-30 strokes with a tight pestle. The lysate was kept on ice for 20 min and centrifuged at 16,000 rcf for 20 min at 4°C. The supernatant was filtered with pre-chilled 0.45 μm filter and incubated with 50 μl of packed Pierce Control Agarose Resin (Thermo Fisher Scientific, Cat# 26150) for 30 min at 4°C with rotation to minimize unspecific binding. The lysate was then incubated with 20 μl of packed GFP-Trap Agarose (Bulldog Bio, Cat# GTA020) for 2 hrs at 4°C with rotation. After binding, the GFP beads were washed 5 times with 1 ml DLB containing 0.5% (v/v) IGEPAL and 10 μM MG132, followed by addition of 40 μl of 4x SDS sample buffer and heating at 95°C for 6 min. The samples were then assessed by silver staining and the protein samples for mass spectrometry were prepared and submitted as above.

Mass Spectrometry and data analysis

In-gel trypsin digestion and liquid chromatography/tandem mass spectrometry (nanoLC-MS/MS) were performed by Taplin Mass Spectrometry Facility at Harvard Medical School. Mass spectrometry results from two gel pieces for each sample were combined, and the results from the experimental and control samples were analyzed with Significance Analysis of INTeractome (SAINT) (v2.5.0) using the total peptides identified for each protein (Choi *et al.*, 2011). Any protein with the SAINT score (average probability) ≥ 0.8 was considered as a high-confidence interactor and was included in the interactome. SAINT analysis included the following numbers of samples: Yki-SBP, four experiments and four controls; Yki-EGFP, three experiments and five controls; Bon-SBP, two experiments and three controls.

Yki protein interactome. Yki protein interactors with SAINT score ≥ 0.8 either in S2 cells or in embryos were included in the Yki protein interactome. The Yki protein interactome was further populated with the interactions incorporated from the STRING database (v11.0) and FlyBase (vFB2020_04) (Szklarczyk *et al.*, 2019; Thurmond *et al.*, 2019). All proteins in the Yki interactome from the current study were imported into the STRING database and analyzed with default settings: full network, medium confidence 0.4 and all active interaction sources (Textmining, Experiments, Databases, Co-expression, Neighborhood, Gene Fusion and Co-occurrence). The summary of physical interactions of Yki in FlyBase was selected to show neighbor-neighbor interactions, and the summary of genetic interactions was selected to show both suppression and enhancement. The interaction data from FlyBase were exported through esyN (Bean et al., 2014), while only the interactions between the proteins that were identified as components of the Yki protein interactome from the current study were incorporated into the Yki protein interactome. The Yki protein interactome was visualized with Cytoscape (Shannon et al., 2003). Nodes represent Yki and Yki interactors identified in the current study. Edges represent the interactions incorporated from STRING and FlyBase. Clustering was done manually based on FlyBase annotations and publications (Thurmond *et al.*, 2019). Gene symbols were updated to FlyBase version FB2020_04, released Aug 18, 2020.

Bon protein interactome. Bon protein interactors with SAINT score ≥ 0.8 from S2 cells were included in the Bon protein interactome which was visualized with Cytoscape. The nodes and edges represent the interactors and interactions identified in the current study, respectively. Gene symbols were updated to FlyBase version FB2020_04, released Aug 18, 2020.

Co-Immunoprecipitation

S2 cells were transfected with indicated plasmids or blank pMT-V5-His vector (Invitrogen, Cat# V412020) using the Effectene transfection reagent (Qiagen, Cat# 301427). 24 hrs after transfection, cells were induced with 0.35 mM $CuSO_4$ overnight at 25°C, collected and lysed on ice for 20 min with 600 µl of ice-cold DLB. The lysate was centrifuged at 16,000 rcf for 20 min at 4°C. 40 µl supernatant was mixed with 20 µl of 4x SDS sample buffer and heated at 95°C for 6 min to generate lysate samples. The rest of the lysate was incubated with 20 µl of packed anti-V5 beads (Sigma-Aldrich, Cat# A7345) or anti-HA beads (Sigma-Aldrich, Cat# E6779) for 2 hrs at 4°C. The beads were then washed 3 times with 1 ml DLB, mixed with 40 µl of 4x SDS sample buffer, and heated at 95°C for 6 min to generate IP samples. The lysate samples and IP samples were subjected to SDS-PAGE followed by western blot using Odyssey Blocking Buffer (PBS) (LI-COR Biosciences, Cat# 927-40003) as blocking buffer, mouse anti-V5 antibody (1:1000, Sigma-Aldrich, Cat# V8012) and Rabbit anti-HA antibody (1:1000, Sigma-Aldrich, Cat# H6908) as primary antibody, and Goat anti-Mouse IgG (1:20,000, LI-COR Biosciences, Cat# 926-68070) and Donkey anti-Rabbit IgG (1:20,000, LI-COR Biosciences, Cat# 926-32213) as secondary antibody. Blotting membranes were scanned with LI-COR Odyssey CLx Imaging Systems.

Immunostaining and fluorescence microscopy

Antibodies. All antibodies and phalloidin reagents used in this study are listed in the Key Resources Table. All primary antibodies from DSHB were used at 1:50 (v/v) dilution. All secondary antibodies from Thermo Fisher Scientific were used at 1:500 (v/v) dilution. Guinea Pig anti-Bon antibody was used at 1: 5000 (v/v) dilution (Beckstead *et al.*, 2001). Guinea Pig anti-Hth antibody was used at 1:1000 (v/v) dilution (personal communication, Claude Desplan Lab). Phalloidin reagents were used at 1:500 (v/v) dilution to detect F-actin.

Embryo staining. Stage 16 embryos were collected and dechorionated with 50% (v/v) Clorox bleach, rinsed with water, and fixed in 20 ml of fixative containing 4% (v/v) formaldehyde (Electron Microscopy Sciences, Cat# 15710), 25% (v/v) Heptane and 1x PBS for 20 min at RT. 8 ml of methanol was added to remove the vitelline membrane. Fixed and devitellinized embryos were washed three times with 1.4 ml methanol, four times with 1.4 ml ethanol and twice with PBT (1x PBS containing 0.1% (v/v) Tween 20). Embryos were subsequently incubated in 1 ml of blocking solution (1:1 (v/v) of Western Blocking Reagent (Roche, Cat#11921681001) and PBT) for 2 hrs at RT and incubated overnight in 500 µl of blocking solution containing 22C10 primary antibody (DSHB, Cat# 22c10) at 4°C. Embryos were then washed five times with 0.1% BSA (m/v in PBT) and incubated in 1 ml of blocking solution for 1 hr at RT. The embryos were then incubated in secondary antibody diluted in blocking solution for 2 hrs in the dark at RT, washed sequentially in 0.1% BSA, PBT and 1x PBS, and mounted with ProLong Gold Antifade Mountant with DAPI (Thermo Fisher Scientific, Cat# P36931). All the incubation and washing were carried out on a nutator.

L3 imaginal disc staining. 3rd instar larval wing discs and eye-antennal discs were dissected in ice-cold 1x PBS and were fixed in 4% (v/v) formaldehyde (Sigma-Aldrich, Cat# F8775) for 15-20

min at RT. The discs were washed with 1x PBS, permeabilized with PB-Triton (1x PBS containing 0.3% (v/v) Triton X-100) for 20 min at RT and were incubated in primary antibodies diluted in blocking solution (1:1 (v/v) of Western Blocking Reagent and PBT) overnight at RT. The discs were then washed four times with PBT, incubated in secondary antibodies diluted in blocking solution for 2-3 hrs in the dark at RT, washed four times with PBT, and mounted with ProLong Gold Antifade Mountant with DAPI. All the incubation and washing steps were carried out on a platform shaker with mild shaking.

Pupal eye staining. Pupal eye staging, dissection and staining procedures were adapted from (Hsiao et al., 2012; Walther and Pichaud, 2006). Newly formed white pupae were circled on the fly vial. 32-44 hrs after puparium formation (APF), pupal eyes were dissected with forceps in ice-cold 1x PBS, transferred to 4% (v/v) formaldehyde (Sigma-Aldrich, Cat# F8775) and fixed for 15-20 min at RT. Fixative was replaced with 1x PBS and washed two times followed by permeabilizing with PB-Triton for 30 min. The pupal eyes were then incubated in primary antibodies diluted in PB-Triton overnight at RT, washed four times with PB-Triton, and incubated in secondary antibody or Phalloidin diluted in PB-Triton for 3 hrs at RT. The pupal eyes were then washed four times with PB-Triton and mounted with ProLong Gold Antifade Mountant with DAPI. All the incubation and washing steps were carried out on a platform shaker with mild shaking.

Fluorescence microscopy. Fluorescent images were acquired using Zeiss LSM 880 Confocal Microscope. For embryo imaging, 20x objective and 1 Airy Unit (AU) pinhole were used. For L3 wing disc imaging, 20x objective was used to take a z stack, and maximum intensity projection of the entire disc was performed to generate final images. For L3 eye-antennal disc imaging, 20x objective and 1 AU were used to take z stacks with optimal step size, and maximum intensity projection was performed for the entire layer of disc proper except for the anti-Ct staining, which was focused on the disc proper while minimizing the inclusion of the focal plane of cone cells. For the F-actin staining in the pupal eye, 63x oil-immersion objective and 1 AU pinhole were used with focal plane set to the apical surface. Images were processed with Fiji (Schindelin et al., 2012).

Bright-field microscopy

Adult eye images were taken under Zeiss Stemi 2000-C Microscope with an attached-on camera at 50x magnification. Adult wings were separated, immersed briefly in isopropanol, mounted with 3:1 (v/v) CMCP-10 (Polysciences, Inc., Cat# 16300-250) and lactic acid, and imaged with Olympus BX60 Microscope under 4x and 40x objectives for the entire wing and wing trichomes, respectively. Due to the difference in size and expression level (dosage compensation of X chromosome driver), only images from female adult flies were analyzed. Images were processed with Fiji.

Scanning electron microscopy (SEM)

Preparation of adult flies for SEM was adapted from (Pepple et al., 2007; Wolff, 2011). 1-2 days old adult flies were sequentially dehydrated in 1 ml of 25%, 50%, 75%, 100%, 100% and 100% ethanol (v/v in water) for 8-16 hrs per step at RT (overnight for the first step). The flies were then

chemically dried in 500 µl of 25%, 50%, 75%, 100%, 100% and 100% Hexamethyldisilazane (v/v in ethanol) (HMDS, Electron Microscopy Sciences, Cat# 16700) for 30 min per step at RT. Most of the HMDS was then removed and the remaining HMDS was allowed to be dried under vacuum in a desiccator containing Indicating Drierite (W.A. Hammond, Cat# 23005) overnight at RT. The samples were then mounted on Aluminum Mount using Carbon Adhesive Tape, and stored in Mount Holder (Electron Microscopy Sciences, Cat# 75220, 77816 and 76510). The samples were subsequently coated with gold at 50 mAmps for 150 secs with Denton Vacuum Desk V sputter coater. Images were acquired with JEOL JSM-6010LA IntouchScope Scanning Electron Microscope using 20 kV voltage, 10 mm working distance and 150x, 300x and 1000x magnifications for an entire eye, zoomed-in view for ectopic antenna, and zoomed-in view for trichomes, respectively. Images were processed with Fiji. The numbers of trichomes were counted with Fiji in an area of 1306 μm^2 (41.73 µm x 31.30 µm) per image for all genotypes.

Total RNA preparation

Pupal eyes were dissected from 40-41 hrs APF pupae (staged for 40 hrs at 25°C and dissected within 1 hr at RT) in ice cold RNase-free 1x PBS diluted from RNase-free 10x PBS (Fisher Scientific, Cat# BP3994) with RNase-free water (Thermo Fisher Scientific, Cat# 10977015). Dissected pupal eyes were immediately transferred to 100 µl of TRIzol (Thermo Fisher Scientific, Cat# 15596026) and kept at RT for 5 min to lyse. Samples in TRIzol were stored at -80°C until 60 pupal eyes for each genotype were collected. All TRIzol samples for each genotype were then thawed and combined, and the volume was brought up to 500 µl per sample. Total RNA was extracted twice by adding 100 µl of chloroform, vigorously shaking for 15 secs, incubating at RT for 3 min, centrifuging at 11,000 rcf at 4°C for 15 min, and collecting the aqueous phase. The total RNA was then precipitated by adding 1 volume of 70% ethanol (v/v in RNase-free water), and purified with RNeasy Mini Kit (QIAGEN, Cat# 74104, 79254).

RNA-sequencing and data analysis

The RNA-seq libraries were prepared from 100 µg of total RNA per genotype with NEBNext Ultra II RNA Library Prep Kit mRNA Isolation Module (NEB, Cat# E7775S, E7490S, E7500S). Quality control and sequencing of the RNA-seq libraries were performed by GENEWIZ, Inc. using Agilent TapeStation and Illumina HiSeq 4000 with a 2x150 paired-end configuration.

The adapter sequences were trimmed from raw reads, and reads shorter than 18 nt were removed by Cutadapt (v2.9) (Martin, 2011). The reads mapped to tRNAs, rRNA, snRNA and snoRNA were removed by mapping through Bowtie 2 (v2.3.5.1) with very sensitive setting and maximum fragment size of 1000 in addition to default setting (Langmead and Salzberg, 2012). The tRNA, rRNA, snRNA and snoRNA reference sequences were obtained from FlyBase (dmel-all-tRNA-r6.33.fasta and dmel-all-miscRNA-r6.33.fasta) (Thurmond *et al.*, 2019). The remaining reads were mapped to *D. melanogaster* genome Ensembl_BDGP6 (Flicek et al., 2014) by STAR (v2.7.0e) (Dobin et al., 2013) with default parameters. Gene counting was achieved by featureCounts (Subread v1.6.2) with overlapping or polycistronic genes counted as a fraction (Liao et al., 2014). Differential gene expression analysis was performed with DEseq2 (v1.30.1) through DEBrowser (v1.16.3) with default settings (Kucukural et al., 2019; Love *et al.*, 2014),

and genes with maximum count fewer than 10 were filtered out. Normalization method used in DESeq2 was Median Ratio Normalization (MRN) (Maza et al., 2013).

The Pearson Correlation Coefficient analysis was performed by ggpubr R package. The Gene Ontology (GO) analysis was performed with DAVID Bioinformatics Resources (v6.8) (Huang da et al., 2009a; b). The ChIP-seq results of Yki, Bon and Svb, and DamID-seq result of Sd on joint target genes of Bon and Yki were analyzed using published data GSE38594, GSE25921, GSE48791 and GSE120731, and visualized with Integrative Genomics Viewer (IGV) (v2.8.2) (Menoret *et al.*, 2013; Negre *et al.*, 2011; Oh *et al.*, 2013; Robinson et al., 2011; Vissers *et al.*, 2018).

qRT-PCR

cDNA was generated from total RNA using SuperScript III First-Strand Synthesis System (Thermo Fisher Scientific, Cat# 18080051). qRT-PCR was performed with biological and technical triplicates using PowerUp SYBR Green Master Mix (Thermo Fisher Scientific, Cat# A25742) on QuantStudio 3 Real-Time PCR System. Gene expression was normalized to ribosomal protein *rp49*. The sequences of the primers are listed in the Key Resources Table.

Quantification and statistical analysis

Statistical significance of phenotype penetrance was determined by Fisher's exact test with two-sided p value calculation using GraphPad Prism (v9.1.0). In all other statistical analyses, data were presented as mean ± SEM of at least three replicates, and the significance was determined by unpaired t-test with Welch's correction and assuming Gaussian distribution using GraphPad Prism (v9.1.0). The numbers (n) and values of each sample used per experiment are provided in Table S5. The p values are presented as follows: not significant, ns ($p > 0.05$), * ($p \leq 0.05$), ** ($p \leq 0.01$), *** ($p \leq 0.001$), **** ($p \leq 0.0001$).

Data and code availability

The RNA-seq datasets generated in this study have been deposited in NCBI's Gene Expression Omnibus (Edgar et al., 2002) and are accessible through GEO Series accession number GSE181299. The mass spectrometry proteomics data have been deposited to the ProteomeXchange Consortium via the PRIDE (Perez-Riverol et al., 2019) partner repository with the dataset identifier PXD027934.

References

Allton, K., Jain, A.K., Herz, H.M., Tsai, W.W., Jung, S.Y., Qin, J., Bergmann, A., Johnson, R.L., and Barton, M.C. (2009). Trim24 targets endogenous p53 for degradation. Proc Natl Acad Sci U S A *106*, 11612-11616. 10.1073/pnas.0813177106.

Andrews, J., Garcia-Estefania, D., Delon, I., Lu, J., Mevel-Ninio, M., Spierer, A., Payre, F., Pauli, D., and Oliver, B. (2000). OVO transcription factors function antagonistically in the Drosophila female germline. Development *127*, 881-892.

Arif, S., Kittelmann, S., and McGregor, A.P. (2015). From shavenbaby to the naked valley: trichome formation as a model for evolutionary developmental biology. Evol Dev *17*, 120-126. 10.1111/ede.12113.
Badouel, C., Gardano, L., Amin, N., Garg, A., Rosenfeld, R., Le Bihan, T., and McNeill, H. (2009). The FERM-domain protein Expanded regulates Hippo pathway activity via direct interactions with the transcriptional activator Yorkie. Dev Cell *16*, 411-420. 10.1016/j.devcel.2009.01.010.
Barish, S., Li, Q., Pan, J.W., Soeder, C., Jones, C., and Volkan, P.C. (2017). Transcriptional profiling of olfactory system development identifies distal antenna as a regulator of subset of neuronal fates. Sci Rep *7*, 40873. 10.1038/srep40873.
Bean, D.M., Heimbach, J., Ficorella, L., Micklem, G., Oliver, S.G., and Favrin, G. (2014). esyN: network building, sharing and publishing. PLoS One *9*, e106035. 10.1371/journal.pone.0106035.
Beckstead, R., Ortiz, J.A., Sanchez, C., Prokopenko, S.N., Chambon, P., Losson, R., and Bellen, H.J. (2001). Bonus, a Drosophila homolog of TIF1 proteins, interacts with nuclear receptors and can inhibit betaFTZ-F1-dependent transcription. Mol Cell *7*, 753-765.
Beckstead, R.B., Ner, S.S., Hales, K.G., Grigliatti, T.A., Baker, B.S., and Bellen, H.J. (2005). Bonus, a Drosophila TIF1 homolog, is a chromatin-associated protein that acts as a modifier of position-effect variegation. Genetics *169*, 783-794. 10.1534/genetics.104.037085.
Betz, A., Lampen, N., Martinek, S., Young, M.W., and Darnell, J.E., Jr. (2001). A Drosophila PIAS homologue negatively regulates stat92E. Proc Natl Acad Sci U S A *98*, 9563-9568. 10.1073/pnas.171302098.
Beyer, T.A., Weiss, A., Khomchuk, Y., Huang, K., Ogunjimi, A.A., Varelas, X., and Wrana, J.L. (2013). Switch enhancers interpret TGF-beta and Hippo signaling to control cell fate in human embryonic stem cells. Cell Rep *5*, 1611-1624. 10.1016/j.celrep.2013.11.021.
Bischof, J., Maeda, R.K., Hediger, M., Karch, F., and Basler, K. (2007). An optimized transgenesis system for Drosophila using germ-line-specific phiC31 integrases. Proc Natl Acad Sci U S A *104*, 3312-3317. 10.1073/pnas.0611511104.
Blochlinger, K., Jan, L.Y., and Jan, Y.N. (1993). Postembryonic patterns of expression of cut, a locus regulating sensory organ identity in Drosophila. Development *117*, 441-450.
Boedigheimer, M., and Laughon, A. (1993). Expanded: a gene involved in the control of cell proliferation in imaginal discs. Development *118*, 1291-1301.
Bohere, J., Mancheno-Ferris, A., Al Hayek, S., Zanet, J., Valenti, P., Akino, K., Yamabe, Y., Inagaki, S., Chanut-Delalande, H., Plaza, S., et al. (2018). Shavenbaby and Yorkie mediate Hippo signaling to protect adult stem cells from apoptosis. Nat Commun *9*, 5123. 10.1038/s41467-018-07569-0.
Borggrefe, T., and Oswald, F. (2009). The Notch signaling pathway: transcriptional regulation at Notch target genes. Cell Mol Life Sci *66*, 1631-1646. 10.1007/s00018-009-8668-7.
Cagan, R.L., and Ready, D.F. (1989). Notch is required for successive cell decisions in the developing Drosophila retina. Genes Dev *3*, 1099-1112. 10.1101/gad.3.8.1099.
Cammas, F., Khetchoumian, K., Chambon, P., and Losson, R. (2012). TRIM involvement in transcriptional regulation. Adv Exp Med Biol *770*, 59-76. 10.1007/978-1-4614-5398-7_5.
Chanut-Delalande, H., Fernandes, I., Roch, F., Payre, F., and Plaza, S. (2006). Shavenbaby couples patterning to epidermal cell shape control. PLoS Biol *4*, e290. 10.1371/journal.pbio.0040290.

Chanut-Delalande, H., Hashimoto, Y., Pelissier-Monier, A., Spokony, R., Dib, A., Kondo, T., Bohere, J., Niimi, K., Latapie, Y., Inagaki, S., et al. (2014). Pri peptides are mediators of ecdysone for the temporal control of development. Nat Cell Biol *16*, 1035-1044. 10.1038/ncb3052.
Choi, H., Larsen, B., Lin, Z.Y., Breitkreutz, A., Mellacheruvu, D., Fermin, D., Qin, Z.S., Tyers, M., Gingras, A.C., and Nesvizhskii, A.I. (2011). SAINT: probabilistic scoring of affinity purification-mass spectrometry data. Nat Methods *8*, 70-73. 10.1038/nmeth.1541.
Couturier, L., Mazouni, K., Corson, F., and Schweisguth, F. (2019). Regulation of Notch output dynamics via specific E(spl)-HLH factors during bristle patterning in Drosophila. Nat Commun *10*, 3486. 10.1038/s41467-019-11477-2.
Davis, J.R., and Tapon, N. (2019). Hippo signalling during development. Development *146*. 10.1242/dev.167106.
Delon, I., Chanut-Delalande, H., and Payre, F. (2003). The Ovo/Shavenbaby transcription factor specifies actin remodelling during epidermal differentiation in Drosophila. Mech Dev *120*, 747-758. 10.1016/s0925-4773(03)00081-9.
Dobin, A., Davis, C.A., Schlesinger, F., Drenkow, J., Zaleski, C., Jha, S., Batut, P., Chaisson, M., and Gingeras, T.R. (2013). STAR: ultrafast universal RNA-seq aligner. Bioinformatics *29*, 15-21. 10.1093/bioinformatics/bts635.
Dominguez, M., and Casares, F. (2005). Organ specification-growth control connection: new in-sights from the Drosophila eye-antennal disc. Dev Dyn *232*, 673-684. 10.1002/dvdy.20311.
Edgar, R., Domrachev, M., and Lash, A.E. (2002). Gene Expression Omnibus: NCBI gene expression and hybridization array data repository. Nucleic Acids Res *30*, 207-210. 10.1093/nar/30.1.207.
Ellis, M.C., O'Neill, E.M., and Rubin, G.M. (1993). Expression of Drosophila glass protein and evidence for negative regulation of its activity in non-neuronal cells by another DNA-binding protein. Development *119*, 855-865.
Fang, X., and Adler, P.N. (2010). Regulation of cell shape, wing hair initiation and the actin cytoskeleton by Trc/Fry and Wts/Mats complexes. Dev Biol *341*, 360-374. 10.1016/j.ydbio.2010.02.029.
Flicek, P., Amode, M.R., Barrell, D., Beal, K., Billis, K., Brent, S., Carvalho-Silva, D., Clapham, P., Coates, G., Fitzgerald, S., et al. (2014). Ensembl 2014. Nucleic Acids Res *42*, D749-755. 10.1093/nar/gkt1196.
Fujii, S., Yavuz, A., Slone, J., Jagge, C., Song, X., and Amrein, H. (2015). Drosophila sugar receptors in sweet taste perception, olfaction, and internal nutrient sensing. Curr Biol *25*, 621-627. 10.1016/j.cub.2014.12.058.
Goodrich, J.S., Clouse, K.N., and Schupbach, T. (2004). Hrb27C, Sqd and Otu cooperatively regulate gurken RNA localization and mediate nurse cell chromosome dispersion in Drosophila oogenesis. Development *131*, 1949-1958. 10.1242/dev.01078.
Hamaratoglu, F., Willecke, M., Kango-Singh, M., Nolo, R., Hyun, E., Tao, C., Jafar-Nejad, H., and Halder, G. (2006). The tumour-suppressor genes NF2/Merlin and Expanded act through Hippo signalling to regulate cell proliferation and apoptosis. Nat Cell Biol *8*, 27-36. 10.1038/ncb1339.
Hari, K.L., Cook, K.R., and Karpen, G.H. (2001). The Drosophila Su(var)2-10 locus regulates chromosome structure and function and encodes a member of the PIAS protein family. Genes Dev *15*, 1334-1348. 10.1101/gad.877901.

Hay, B.A., Wolff, T., and Rubin, G.M. (1994). Expression of baculovirus P35 prevents cell death in Drosophila. Development *120*, 2121-2129.
He, L., Yuan, L., Yu, W., Sun, Y., Jiang, D., Wang, X., Feng, X., Wang, Z., Xu, J., Yang, R., et al. (2020). A Regulation Loop between YAP and NR4A1 Balances Cell Proliferation and Apoptosis. Cell Rep *33*, 108284. 10.1016/j.celrep.2020.108284.
He, Y., Emoto, K., Fang, X., Ren, N., Tian, X., Jan, Y.N., and Adler, P.N. (2005). Drosophila Mob family proteins interact with the related tricornered (Trc) and warts (Wts) kinases. Mol Biol Cell *16*, 4139-4152. 10.1091/mbc.e05-01-0018.
Hergovich, A., and Hemmings, B.A. (2012). Hippo signalling in the G2/M cell cycle phase: lessons learned from the yeast MEN and SIN pathways. Semin Cell Dev Biol *23*, 794-802. 10.1016/j.semcdb.2012.04.001.
Hoge, M.A. (1915). Another Gene in the Fourth Chromosome of Drosophila. The American Naturalist *49*, 47-49.
Hsiao, H.Y., Johnston, R.J., Jr., Jukam, D., Vasiliauskas, D., Desplan, C., and Rister, J. (2012). Dissection and immunohistochemistry of larval, pupal and adult Drosophila retinas. J Vis Exp, 4347. 10.3791/4347.
Huang da, W., Sherman, B.T., and Lempicki, R.A. (2009a). Bioinformatics enrichment tools: paths toward the comprehensive functional analysis of large gene lists. Nucleic Acids Res *37*, 1-13. 10.1093/nar/gkn923.
Huang da, W., Sherman, B.T., and Lempicki, R.A. (2009b). Systematic and integrative analysis of large gene lists using DAVID bioinformatics resources. Nat Protoc *4*, 44-57. 10.1038/nprot.2008.211.
Huang, J., Wu, S., Barrera, J., Matthews, K., and Pan, D. (2005). The Hippo signaling pathway coordinately regulates cell proliferation and apoptosis by inactivating Yorkie, the Drosophila Homolog of YAP. Cell *122*, 421-434. 10.1016/j.cell.2005.06.007.
Isbel, L., Srivastava, R., Oey, H., Spurling, A., Daxinger, L., Puthalakath, H., and Whitelaw, E. (2015). Trim33 Binds and Silences a Class of Young Endogenous Retroviruses in the Mouse Testis; a Novel Component of the Arms Race between Retrotransposons and the Host Genome. PLoS Genet *11*, e1005693. 10.1371/journal.pgen.1005693.
Ito, H., Sato, K., Koganezawa, M., Ote, M., Matsumoto, K., Hama, C., and Yamamoto, D. (2012). Fruitless recruits two antagonistic chromatin factors to establish single-neuron sexual dimorphism. Cell *149*, 1327-1338. 10.1016/j.cell.2012.04.025.
Jukam, D., Xie, B., Rister, J., Terrell, D., Charlton-Perkins, M., Pistillo, D., Gebelein, B., Desplan, C., and Cook, T. (2013). Opposite feedbacks in the Hippo pathway for growth control and neural fate. Science *342*, 1238016. 10.1126/science.1238016.
Kelly, R.D., and Cowley, S.M. (2013). The physiological roles of histone deacetylase (HDAC) 1 and 2: complex co-stars with multiple leading parts. Biochem Soc Trans *41*, 741-749. 10.1042/BST20130010.
Kerber, B., Monge, I., Mueller, M., Mitchell, P.J., and Cohen, S.M. (2001). The AP-2 transcription factor is required for joint formation and cell survival in Drosophila leg development. Development *128*, 1231-1238.
Kim, M., Kim, T., Johnson, R.L., and Lim, D.S. (2015). Transcriptional co-repressor function of the hippo pathway transducers YAP and TAZ. Cell Rep *11*, 270-282. 10.1016/j.celrep.2015.03.015.

Knust, E., Schrons, H., Grawe, F., and Campos-Ortega, J.A. (1992). Seven genes of the Enhancer of split complex of Drosophila melanogaster encode helix-loop-helix proteins. Genetics *132*, 505-518.
Kucukural, A., Yukselen, O., Ozata, D.M., Moore, M.J., and Garber, M. (2019). DEBrowser: interactive differential expression analysis and visualization tool for count data. Bmc Genomics *20*, 6. 10.1186/s12864-018-5362-x.
Kulkarni, A., Chang, M.T., Vissers, J.H.A., Dey, A., and Harvey, K.F. (2020). The Hippo Pathway as a Driver of Select Human Cancers. Trends Cancer *6*, 781-796. 10.1016/j.trecan.2020.04.004.
Kumar, J.P. (2018). The fly eye: Through the looking glass. Dev Dyn *247*, 111-123. 10.1002/dvdy.24585.
Kumar, J.P., and Moses, K. (2001). EGF receptor and Notch signaling act upstream of Eyeless/Pax6 to control eye specification. Cell *104*, 687-697. 10.1016/s0092-8674(01)00265-3.
Kurata, S., Go, M.J., Artavanis-Tsakonas, S., and Gehring, W.J. (2000). Notch signaling and the determination of appendage identity. Proc Natl Acad Sci U S A *97*, 2117-2122. 10.1073/pnas.040556497.
Kwon, Y., Vinayagam, A., Sun, X., Dephoure, N., Gygi, S.P., Hong, P., and Perrimon, N. (2013). The Hippo signaling pathway interactome. Science *342*, 737-740. 10.1126/science.1243971.
Lai, E.C., Bodner, R., and Posakony, J.W. (2000). The enhancer of split complex of Drosophila includes four Notch-regulated members of the bearded gene family. Development *127*, 3441-3455.
Lai, E.C., and Rubin, G.M. (2001). Neuralized is essential for a subset of Notch pathway-dependent cell fate decisions during Drosophila eye development. Proc Natl Acad Sci U S A *98*, 5637-5642. 10.1073/pnas.101135498.
Lai, Z.C., Wei, X., Shimizu, T., Ramos, E., Rohrbaugh, M., Nikolaidis, N., Ho, L.L., and Li, Y. (2005). Control of cell proliferation and apoptosis by mob as tumor suppressor, mats. Cell *120*, 675-685. 10.1016/j.cell.2004.12.036.
Langmead, B., and Salzberg, S.L. (2012). Fast gapped-read alignment with Bowtie 2. Nat Methods *9*, 357-359. 10.1038/nmeth.1923.
Liao, Y., Smyth, G.K., and Shi, W. (2014). featureCounts: an efficient general purpose program for assigning sequence reads to genomic features. Bioinformatics *30*, 923-930. 10.1093/bioinformatics/btt656.
Ligoxygakis, P., Bray, S.J., Apidianakis, Y., and Delidakis, C. (1999). Ectopic expression of individual E(spl) genes has differential effects on different cell fate decisions and underscores the biphasic requirement for notch activity in wing margin establishment in Drosophila. Development *126*, 2205-2214.
Love, M.I., Huber, W., and Anders, S. (2014). Moderated estimation of fold change and dispersion for RNA-seq data with DESeq2. Genome Biol *15*, 550. 10.1186/s13059-014-0550-8.
Mach, J., Atkins, M., Gajewski, K.M., Mottier-Pavie, V., Sansores-Garcia, L., Xie, J., Mills, R.A., Kowalczyk, W., Van Huffel, L., Mills, G.B., and Halder, G. (2018). Modulation of the Hippo pathway and organ growth by RNA processing proteins. Proc Natl Acad Sci U S A *115*, 10684-10689. 10.1073/pnas.1807325115.
Martin, M. (2011). Cutadapt Removes Adapter Sequences From High-Throughput Sequencing Reads. EMBnet.journal *17*, 10-12. 10.14806/ej.17.1.200.

Maza, E., Frasse, P., Senin, P., Bouzayen, M., and Zouine, M. (2013). Comparison of normalization methods for differential gene expression analysis in RNA-Seq experiments: A matter of relative size of studied transcriptomes. Commun Integr Biol *6*, e25849. 10.4161/cib.25849.
McAvera, R.M., and Crawford, L.J. (2020). TIF1 Proteins in Genome Stability and Cancer. Cancers (Basel) *12*. 10.3390/cancers12082094.
McCartney, B.M., Kulikauskas, R.M., LaJeunesse, D.R., and Fehon, R.G. (2000). The neurofibromatosis-2 homologue, Merlin, and the tumor suppressor expanded function together in Drosophila to regulate cell proliferation and differentiation. Development *127*, 1315-1324.
Meng, Z., Moroishi, T., and Guan, K.L. (2016). Mechanisms of Hippo pathway regulation. Genes Dev *30*, 1-17. 10.1101/gad.274027.115.
Menoret, D., Santolini, M., Fernandes, I., Spokony, R., Zanet, J., Gonzalez, I., Latapie, Y., Ferrer, P., Rouault, H., White, K.P., et al. (2013). Genome-wide analyses of Shavenbaby target genes reveals distinct features of enhancer organization. Genome Biol *14*, R86. 10.1186/gb-2013-14-8-r86.
Menuz, K., Larter, N.K., Park, J., and Carlson, J.R. (2014). An RNA-seq screen of the Drosophila antenna identifies a transporter necessary for ammonia detection. PLoS Genet *10*, e1004810. 10.1371/journal.pgen.1004810.
Micchelli, C.A., Rulifson, E.J., and Blair, S.S. (1997). The function and regulation of cut expression on the wing margin of Drosophila: Notch, Wingless and a dominant negative role for Delta and Serrate. Development *124*, 1485-1495.
Milton, C.C., Grusche, F.A., Degoutin, J.L., Yu, E., Dai, Q., Lai, E.C., and Harvey, K.F. (2014). The Hippo pathway regulates hematopoiesis in Drosophila melanogaster. Curr Biol *24*, 2673-2680. 10.1016/j.cub.2014.10.031.
Misra, J.R., and Irvine, K.D. (2018). The Hippo Signaling Network and Its Biological Functions. Annu Rev Genet *52*, 65-87. 10.1146/annurev-genet-120417-031621.
Monge, I., Krishnamurthy, R., Sims, D., Hirth, F., Spengler, M., Kammermeier, L., Reichert, H., and Mitchell, P.J. (2001). Drosophila transcription factor AP-2 in proboscis, leg and brain central complex development. Development *128*, 1239-1252.
Negre, N., Brown, C.D., Ma, L., Bristow, C.A., Miller, S.W., Wagner, U., Kheradpour, P., Eaton, M.L., Loriaux, P., Sealfon, R., et al. (2011). A cis-regulatory map of the Drosophila genome. Nature *471*, 527-531. 10.1038/nature09990.
Ninova, M., Chen, Y.A., Godneeva, B., Rogers, A.K., Luo, Y., Fejes Toth, K., and Aravin, A.A. (2020a). Su(var)2-10 and the SUMO Pathway Link piRNA-Guided Target Recognition to Chromatin Silencing. Mol Cell *77*, 556-570 e556. 10.1016/j.molcel.2019.11.012.
Ninova, M., Godneeva, B., Chen, Y.A., Luo, Y., Prakash, S.J., Jankovics, F., Erdelyi, M., Aravin, A.A., and Fejes Toth, K. (2020b). The SUMO Ligase Su(var)2-10 Controls Hetero- and Euchromatic Gene Expression via Establishing H3K9 Trimethylation and Negative Feedback Regulation. Mol Cell *77*, 571-585 e574. 10.1016/j.molcel.2019.09.033.
Nolo, R., Morrison, C.M., Tao, C., Zhang, X., and Halder, G. (2006). The bantam microRNA is a target of the hippo tumor-suppressor pathway. Curr Biol *16*, 1895-1904. 10.1016/j.cub.2006.08.057.

Oh, H., and Irvine, K.D. (2008). In vivo regulation of Yorkie phosphorylation and localization. Development *135*, 1081-1088. 10.1242/dev.015255.
Oh, H., Slattery, M., Ma, L., Crofts, A., White, K.P., Mann, R.S., and Irvine, K.D. (2013). Genome-wide association of Yorkie with chromatin and chromatin-remodeling complexes. Cell Rep *3*, 309-318. 10.1016/j.celrep.2013.01.008.
Oh, H., Slattery, M., Ma, L., White, K.P., Mann, R.S., and Irvine, K.D. (2014). Yorkie promotes transcription by recruiting a histone methyltransferase complex. Cell Rep *8*, 449-459. 10.1016/j.celrep.2014.06.017.
Ordway, A.J., Teeters, G.M., Weasner, B.M., Weasner, B.P., Policastro, R., and Kumar, J.P. (2021). A multi-gene knockdown approach reveals a new role for Pax6 in controlling organ number in Drosophila. Development *148*. 10.1242/dev.198796.
Pai, C.Y., Kuo, T.S., Jaw, T.J., Kurant, E., Chen, C.T., Bessarab, D.A., Salzberg, A., and Sun, Y.H. (1998). The Homothorax homeoprotein activates the nuclear localization of another homeoprotein, extradenticle, and suppresses eye development in Drosophila. Genes Dev *12*, 435-446. 10.1101/gad.12.3.435.
Pan, D. (2010). The hippo signaling pathway in development and cancer. Dev Cell *19*, 491-505. 10.1016/j.devcel.2010.09.011.
Pepple, K.L., Anderson, A.E., Frankfort, B.J., and Mardon, G. (2007). A genetic screen in Drosophila for genes interacting with senseless during neuronal development identifies the importin moleskin. Genetics *175*, 125-141. 10.1534/genetics.106.065680.
Perez-Riverol, Y., Csordas, A., Bai, J., Bernal-Llinares, M., Hewapathirana, S., Kundu, D.J., Inuganti, A., Griss, J., Mayer, G., Eisenacher, M., et al. (2019). The PRIDE database and related tools and resources in 2019: improving support for quantification data. Nucleic Acids Res *47*, D442-D450. 10.1093/nar/gky1106.
Pojer, J.M., Manning, S.A., Kroeger, B., Kondo, S., and Harvey, K.F. (2021). The Hippo pathway uses different machinery to control cell fate and organ size. iScience *24*, 102830. 10.1016/j.isci.2021.102830.
Robinson, J.T., Thorvaldsdottir, H., Winckler, W., Guttman, M., Lander, E.S., Getz, G., and Mesirov, J.P. (2011). Integrative genomics viewer. Nat Biotechnol *29*, 24-26. 10.1038/nbt.1754.
Rossmann, M.P., Hoi, K., Chan, V., Abraham, B.J., Yang, S., Mullahoo, J., Papanastasiou, M., Wang, Y., Elia, I., Perlin, J.R., et al. (2021). Cell-specific transcriptional control of mitochondrial metabolism by TIF1gamma drives erythropoiesis. Science *372*, 716-721. 10.1126/science.aaz2740.
Salzberg, A., Prokopenko, S.N., He, Y., Tsai, P., Pal, M., Maroy, P., Glover, D.M., Deak, P., and Bellen, H.J. (1997). P-element insertion alleles of essential genes on the third chromosome of Drosophila melanogaster: mutations affecting embryonic PNS development. Genetics *147*, 1723-1741.
Schindelin, J., Arganda-Carreras, I., Frise, E., Kaynig, V., Longair, M., Pietzsch, T., Preibisch, S., Rueden, C., Saalfeld, S., Schmid, B., et al. (2012). Fiji: an open-source platform for biological-image analysis. Nat Methods *9*, 676-682. 10.1038/nmeth.2019.
Schultz, D.C., Friedman, J.R., and Rauscher, F.J., 3rd (2001). Targeting histone deacetylase complexes via KRAB-zinc finger proteins: the PHD and bromodomains of KAP-1 form a cooperative unit that recruits a novel isoform of the Mi-2alpha subunit of NuRD. Genes Dev *15*, 428-443. 10.1101/gad.869501.

Seto, E., and Yoshida, M. (2014). Erasers of histone acetylation: the histone deacetylase enzymes. Cold Spring Harb Perspect Biol *6*, a018713. 10.1101/cshperspect.a018713.
Shannon, P., Markiel, A., Ozier, O., Baliga, N.S., Wang, J.T., Ramage, D., Amin, N., Schwikowski, B., and Ideker, T. (2003). Cytoscape: a software environment for integrated models of biomolecular interaction networks. Genome Res *13*, 2498-2504. 10.1101/gr.1239303.
Szklarczyk, D., Gable, A.L., Lyon, D., Junge, A., Wyder, S., Huerta-Cepas, J., Simonovic, M., Doncheva, N.T., Morris, J.H., Bork, P., et al. (2019). STRING v11: protein-protein association networks with increased coverage, supporting functional discovery in genome-wide experimental datasets. Nucleic Acids Res *47*, D607-D613. 10.1093/nar/gky1131.
Tardi, N.J., Cook, M.E., and Edwards, K.A. (2012). Rapid phenotypic analysis of uncoated Drosophila samples with low-vacuum scanning electron microscopy. Fly (Austin) *6*, 184-192. 10.4161/fly.20525.
Tare, M., Puli, O.R., Moran, M.T., Kango-Singh, M., and Singh, A. (2013). Domain specific genetic mosaic system in the Drosophila eye. Genesis *51*, 68-74. 10.1002/dvg.22355.
Thurmond, J., Goodman, J.L., Strelets, V.B., Attrill, H., Gramates, L.S., Marygold, S.J., Matthews, B.B., Millburn, G., Antonazzo, G., Trovisco, V., et al. (2019). FlyBase 2.0: the next generation. Nucleic Acids Res *47*, D759-D765. 10.1093/nar/gky1003.
Treisman, J.E. (2013). Retinal differentiation in Drosophila. Wiley Interdiscip Rev Dev Biol *2*, 545-557. 10.1002/wdev.100.
Vissers, J.H.A., Froldi, F., Schroder, J., Papenfuss, A.T., Cheng, L.Y., and Harvey, K.F. (2018). The Scalloped and Nerfin-1 Transcription Factors Cooperate to Maintain Neuronal Cell Fate. Cell Rep *25*, 1561-1576 e1567. 10.1016/j.celrep.2018.10.038.
Vosshall, L.B. (2001). The molecular logic of olfaction in Drosophila. Chem Senses *26*, 207-213. 10.1093/chemse/26.2.207.
Walther, R.F., and Pichaud, F. (2006). Immunofluorescent staining and imaging of the pupal and adult Drosophila visual system. Nat Protoc *1*, 2635-2642. 10.1038/nprot.2006.379.
Wang, C.W., and Sun, Y.H. (2012). Segregation of eye and antenna fates maintained by mutual antagonism in Drosophila. Development *139*, 3413-3421. 10.1242/dev.078857.
Weasner, B.M., and Kumar, J.P. (2013). Competition among gene regulatory networks imposes order within the eye-antennal disc of Drosophila. Development *140*, 205-215. 10.1242/dev.085423.
Wittkorn, E., Sarkar, A., Garcia, K., Kango-Singh, M., and Singh, A. (2015). The Hippo pathway effector Yki downregulates Wg signaling to promote retinal differentiation in the Drosophila eye. Development *142*, 2002-2013. 10.1242/dev.117358.
Wodarz, A., Hinz, U., Engelbert, M., and Knust, E. (1995). Expression of crumbs confers apical character on plasma membrane domains of ectodermal epithelia of Drosophila. Cell *82*, 67-76. 10.1016/0092-8674(95)90053-5.
Wolff, T. (2011). Preparation of Drosophila eye specimens for scanning electron microscopy. Cold Spring Harb Protoc *2011*, 1383-1385. 10.1101/pdb.prot066506.
Yang, L., Paul, S., DuBois-Coyne, S., Kyriakakis, P., and Veraksa, A. (2017). Medium-scale Preparation of Drosophila Embryo Extracts for Proteomic Experiments. J Vis Exp. 10.3791/55804.

Yang, L., and Veraksa, A. (2017). Single-Step Affinity Purification of ERK Signaling Complexes Using the Streptavidin-Binding Peptide (SBP) Tag. Methods Mol Biol *1487*, 113-126. 10.1007/978-1-4939-6424-6_8.
Yu, F.X., and Guan, K.L. (2013). The Hippo pathway: regulators and regulations. Genes Dev *27*, 355-371. 10.1101/gad.210773.112.
Zhang, C., Robinson, B.S., Xu, W., Yang, L., Yao, B., Zhao, H., Byun, P.K., Jin, P., Veraksa, A., and Moberg, K.H. (2015). The ecdysone receptor coactivator Taiman links Yorkie to transcriptional control of germline stem cell factors in somatic tissue. Dev Cell *34*, 168-180. 10.1016/j.devcel.2015.05.010.
Zhang, T., Zhou, Q., and Pignoni, F. (2011). Yki/YAP, Sd/TEAD and Hth/MEIS control tissue specification in the Drosophila eye disc epithelium. PLoS One *6*, e22278. 10.1371/journal.pone.0022278.
Zhao, B., Ye, X., Yu, J., Li, L., Li, W., Li, S., Yu, J., Lin, J.D., Wang, C.Y., Chinnaiyan, A.M., et al. (2008). TEAD mediates YAP-dependent gene induction and growth control. Genes Dev *22*, 1962-1971. 10.1101/gad.1664408.
Zheng, Y., and Pan, D. (2019). The Hippo Signaling Pathway in Development and Disease. Dev Cell *50*, 264-282. 10.1016/j.devcel.2019.06.003.

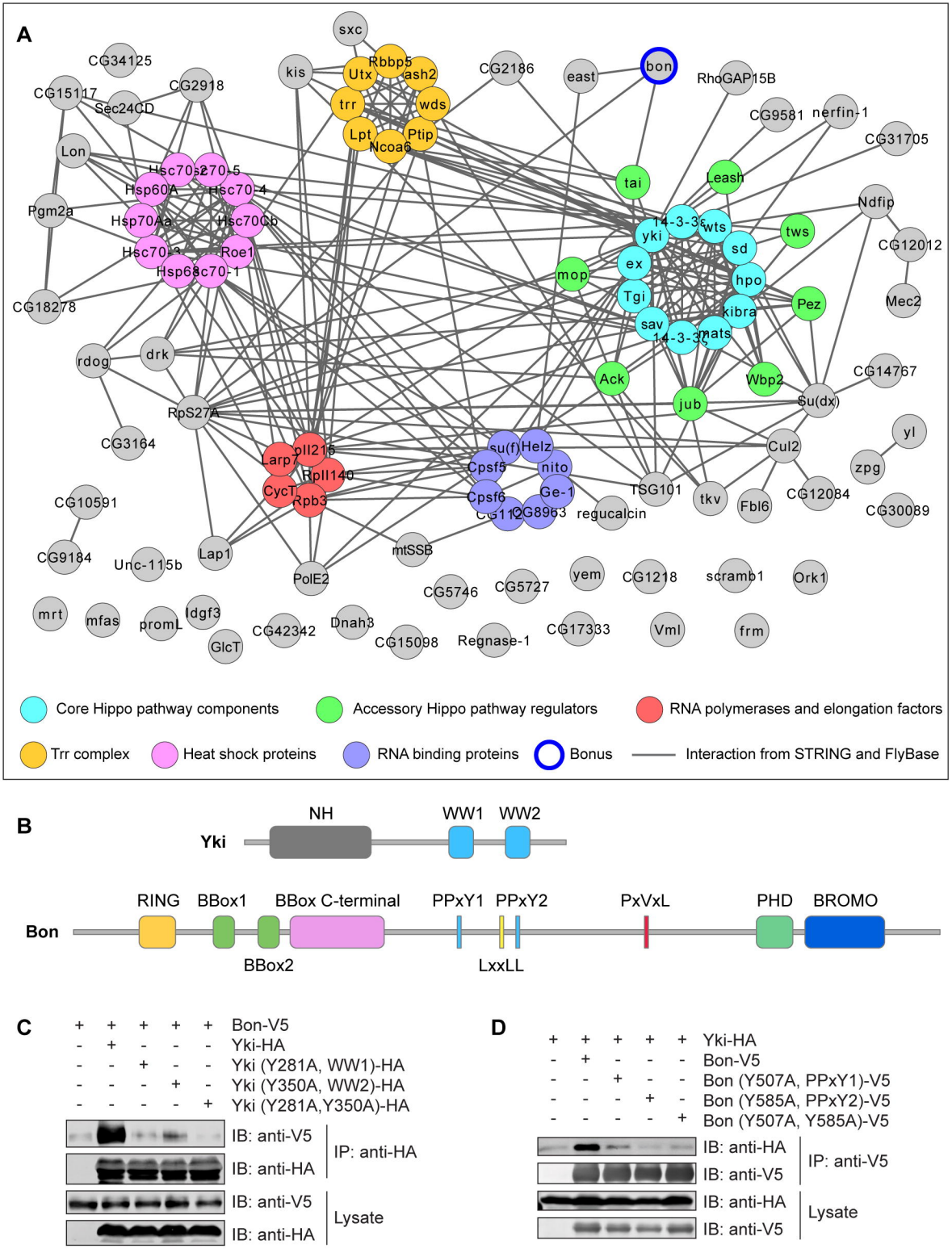
A
sxc
CG34125
kis
Rbbp5
Utx
ash2
CG2186
east
bon
RhoGAP15B
CG15117
CG2918
Sec24CD
trr
wds
CG9581
nerfin-1
Lpt
Ptip
Ncoa6
CG31705
Lon
Hsc70s2
270-5
Hsp60A
Hsc70-4
tai
Leash
Pgm2a
Hsp70Aa
Hsc70Cb
Ndfip
14-3-3ε
wts
yki
tws
Hsc70-3
Roe1
sd
CG12012
Hsp68
c70-1
ex
mop
hpo
Tgi
Pez
Mec2
CG18278
kibra
sav
mats
14-3-3ζ
rdog
drk
Ack
Wbp2
CG14767
jub
Su(dx)
RpS27A
yl
CG3164
su(f)
Helz
Cul2
pII215
Larp7
Cpsf5
nito
zpg
RpII140
CycT
Ge-1
TSG101
tkv
CG12084
CG10591
Rpb3
Cpsf6
Fbl6
CG30089
CG112
CG8963
regucalcin
mtSSB
CG9184
Unc-115b
Lap1
PolE2
yem
CG1218
scramb1
Ork1
CG5746
CG5727
mrt
mfas
promL
Idgf3
CG42342
Dnah3
CG15098
Regnase-1
CG17333
Vml
frm
GlcT
Core Hippo pathway components
Accessory Hippo pathway regulators
RNA polymerases and elongation factors
Trr complex
Heat shock proteins
RNA binding proteins
Bonus
Interaction from STRING and FlyBase
B
Yki
NH
WW1
WW2
Bon
RING
BBox1
BBox C-terminal
PPxY1
PPxY2
PxVxL
PHD
BROMO
BBox2
LxxLL
C
+ + + + + Bon-V5
- + - - - Yki-HA
- - + - - Yki (Y281A, WW1)-HA
- - - + - Yki (Y350A, WW2)-HA
- - - - + Yki (Y281A,Y350A)-HA
IB: anti-V5
IB: anti-HA
IP: anti-HA
IB: anti-V5
IB: anti-HA
Lysate
D
+ + + + + Yki-HA
- + - - - Bon-V5
- - + - - Bon (Y507A, PPxY1)-V5
- - - + - Bon (Y585A, PPxY2)-V5
- - - - + Bon (Y507A, Y585A)-V5
IB: anti-HA
IB: anti-V5
IP: anti-V5
IB: anti-HA
IB: anti-V5
Lysate

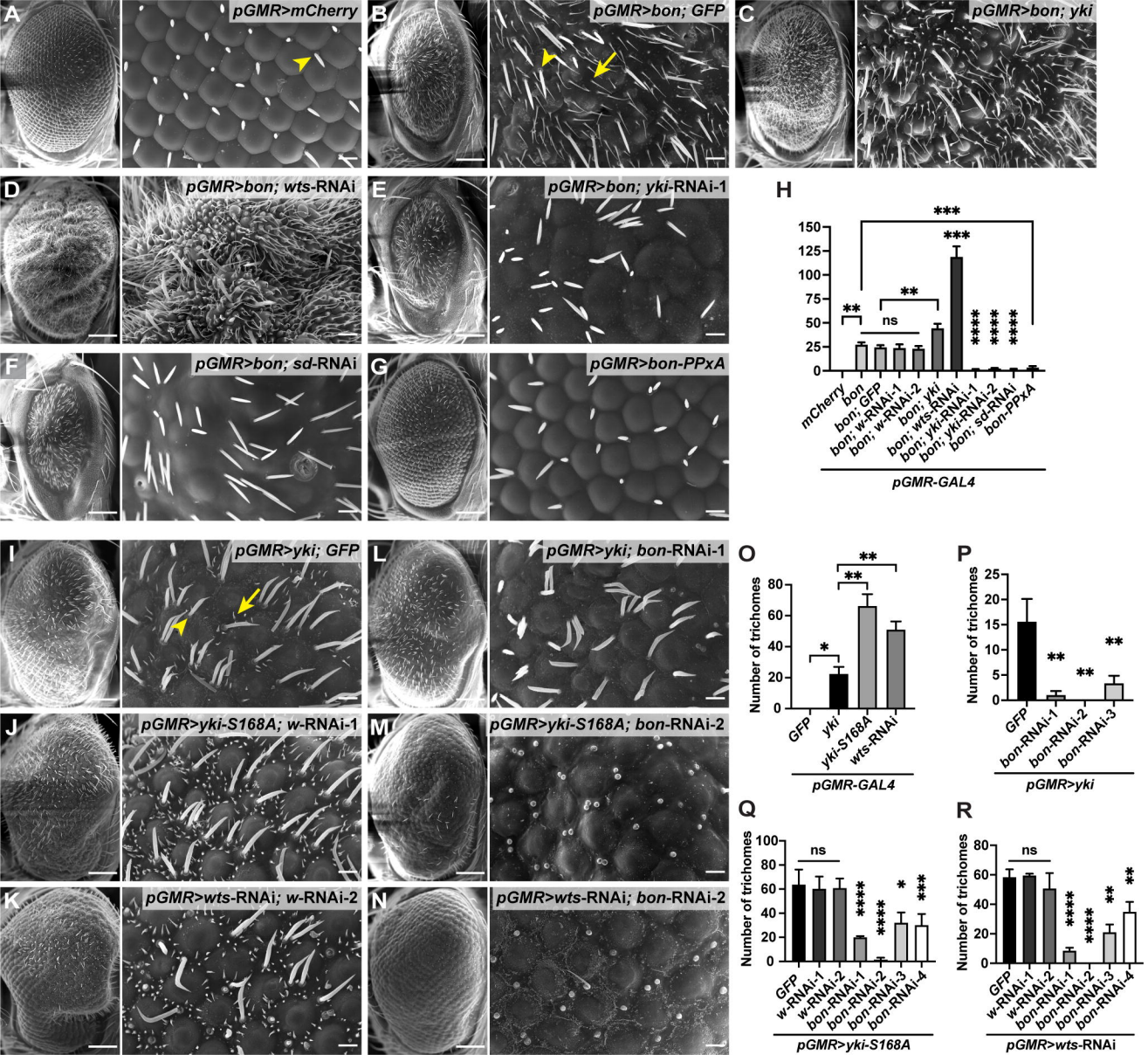
A
pGMR>mCherry
B
pGMR>bon; GFP
C
pGMR>bon; yki
D
pGMR>bon; wts-RNAi
E
pGMR>bon; yki-RNAi-1
F
pGMR>bon; sd-RNAi
G
pGMR>bon-PPxA
H
150
125
100
75
50
25
0
***
***
**
**
ns
****
****
****
mCherry
bon
bon; GFP
bon; w-RNAi-1
bon; w-RNAi-2
bon; yki
bon; wts-RNAi
bon; yki-RNAi-1
bon; yki-RNAi-2
bon; sd-RNAi
bon-PPxA
pGMR-GAL4
I
pGMR>yki; GFP
L
pGMR>yki; bon-RNAi-1
J
pGMR>yki-S168A; w-RNAi-1
M
pGMR>yki-S168A; bon-RNAi-2
K
pGMR>wts-RNAi; w-RNAi-2
N
pGMR>wts-RNAi; bon-RNAi-2
O
Number of trichomes
80
60
40
20
0
*
**
**
GFP
yki
yki-S168A
wts-RNAi
pGMR-GAL4
P
Number of trichomes
25
20
15
10
5
0
**
**
**
GFP
bon-RNAi-1
bon-RNAi-2
bon-RNAi-3
pGMR>yki
Q
Number of trichomes
100
80
60
40
20
0
ns
****
****
*
***
GFP
w-RNAi-1
w-RNAi-2
bon-RNAi-1
bon-RNAi-2
bon-RNAi-3
bon-RNAi-4
pGMR>yki-S168A
R
Number of trichomes
80
60
40
20
0
ns
****
****
**
**
GFP
w-RNAi-1
w-RNAi-2
bon-RNAi-1
bon-RNAi-2
bon-RNAi-3
bon-RNAi-4
pGMR>wts-RNAi

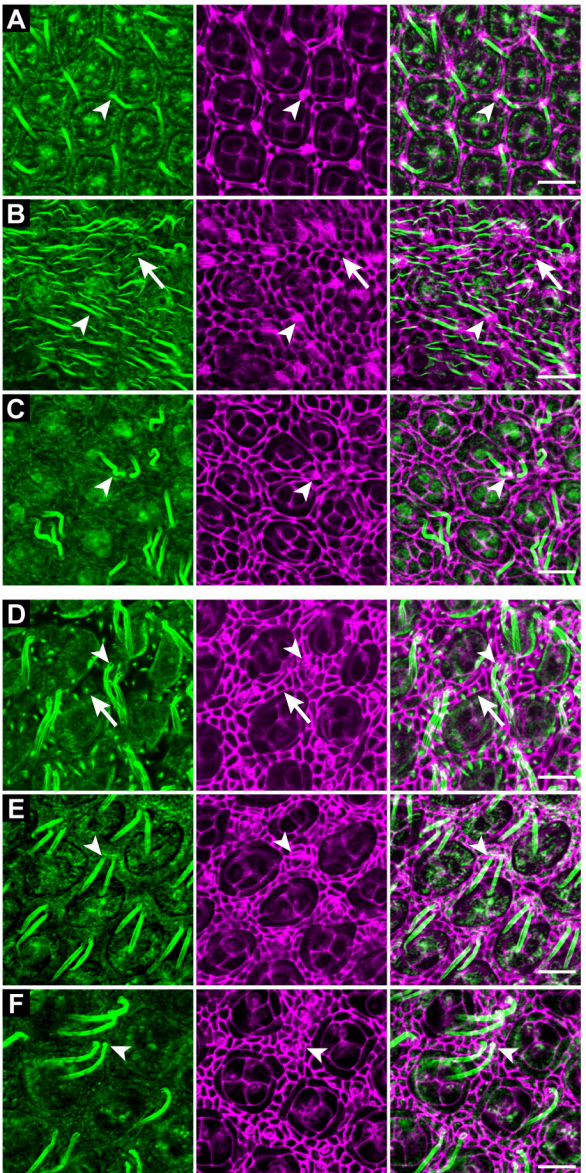
F-Actin
Dlg
F-Actin Dlg
A
pGMR>mCherry
B
pGMR>bon
C
pGMR>bon; yki-RNAi-1
D
pGMR>yki-S168A; GFP
E
pGMR>yki-S168A; bon-RNAi-2
F
pGMR>yki-S168A; bon-RNAi-3

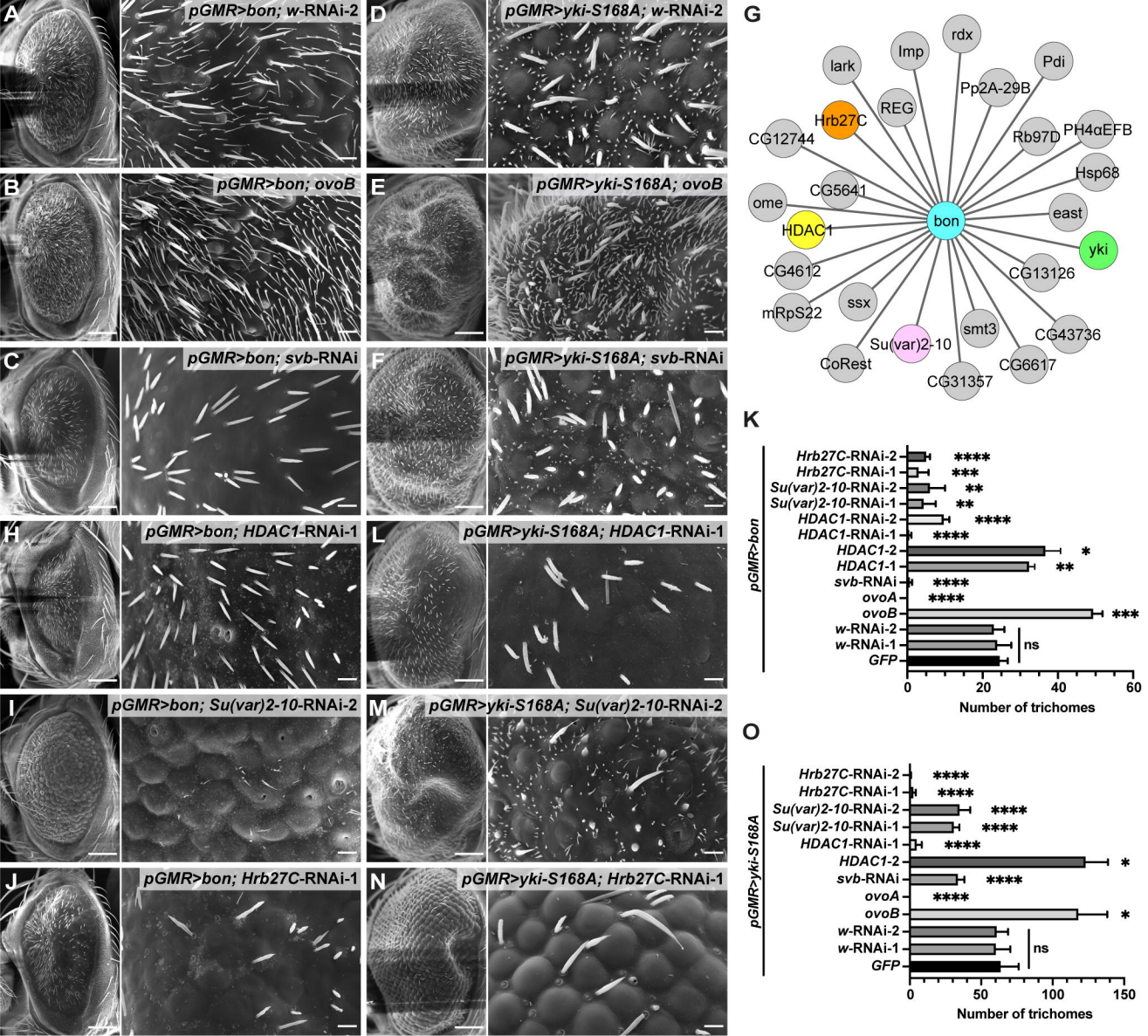
A
pGMR>bon; w-RNAi-2
B
pGMR>bon; ovoB
C
pGMR>bon; svb-RNAi
H
pGMR>bon; HDAC1-RNAi-1
I
pGMR>bon; Su(var)2-10-RNAi-2
J
pGMR>bon; Hrb27C-RNAi-1
D
pGMR>yki-S168A; w-RNAi-2
E
pGMR>yki-S168A; ovoB
F
pGMR>yki-S168A; svb-RNAi
L
pGMR>yki-S168A; HDAC1-RNAi-1
M
pGMR>yki-S168A; Su(var)2-10-RNAi-2
N
pGMR>yki-S168A; Hrb27C-RNAi-1
G
rdx
Imp
lark
Pdi
Pp2A-29B
REG
Hrb27C
CG12744
Rb97D
PH4αEFB
Hsp68
CG5641
ome
bon
east
HDAC1
yki
CG4612
CG13126
ssx
mRpS22
smt3
CG43736
Su(var)2-10
CoRest
CG6617
CG31357
K
pGMR>bon
Hrb27C-RNAi-2
Hrb27C-RNAi-1
Su(var)2-10-RNAi-2
Su(var)2-10-RNAi-1
HDAC1-RNAi-2
HDAC1-RNAi-1
HDAC1-2
HDAC1-1
svb-RNAi
ovoA
ovoB
w-RNAi-2
w-RNAi-1
GFP
****
***
**
**
****
****
*
**
****
****
***
ns
0
20
40
60
Number of trichomes
O
pGMR>yki-S168A
Hrb27C-RNAi-2
Hrb27C-RNAi-1
Su(var)2-10-RNAi-2
Su(var)2-10-RNAi-1
HDAC1-RNAi-1
HDAC1-2
svb-RNAi
ovoA
ovoB
w-RNAi-2
w-RNAi-1
GFP
****
****
****
****
****
*
****
****
*
ns
0
50
100
150
Number of trichomes

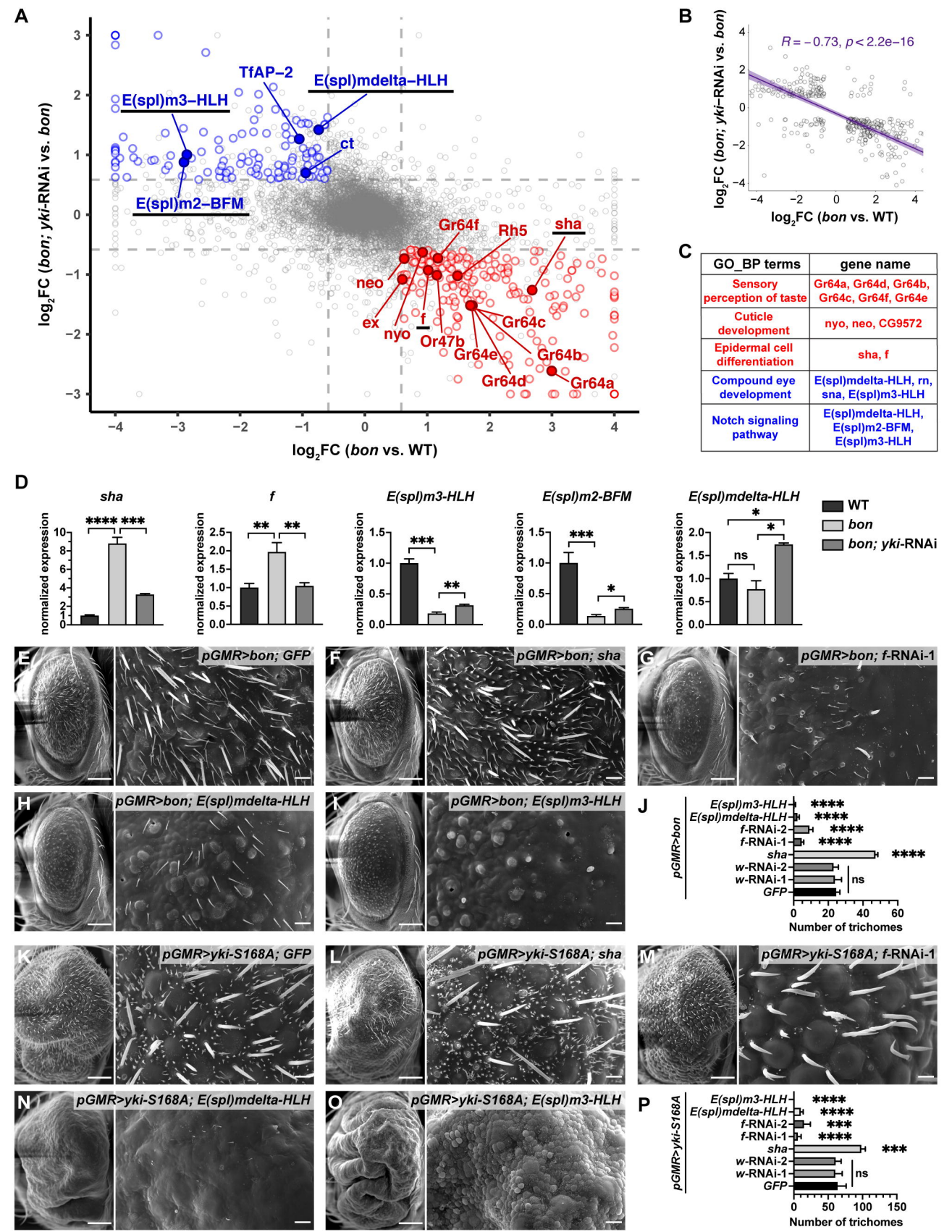
A
log2FC (bon; yki-RNAi vs. bon)
log2FC (bon vs. WT)
E(spl)m3–HLH
TfAP–2
E(spl)mdelta–HLH
ct
E(spl)m2–BFM
Gr64f
Rh5
sha
neo
ex
nyo
f
Or47b
Gr64c
Gr64e
Gr64b
Gr64d
Gr64a
B
R = −0.73, p < 2.2e−16
log2FC (bon; yki-RNAi vs. bon)
log2FC (bon vs. WT)
C
GO_BP terms | gene name
Sensory perception of taste | Gr64a, Gr64d, Gr64b, Gr64c, Gr64f, Gr64e
Cuticle development | nyo, neo, CG9572
Epidermal cell differentiation | sha, f
Compound eye development | E(spl)mdelta-HLH, rn, sna, E(spl)m3-HLH
Notch signaling pathway | E(spl)mdelta-HLH, E(spl)m2-BFM, E(spl)m3-HLH
D
sha
f
E(spl)m3-HLH
E(spl)m2-BFM
E(spl)mdelta-HLH
normalized expression
WT
bon
bon; yki-RNAi
ns
E
pGMR>bon; GFP
F
pGMR>bon; sha
G
pGMR>bon; f-RNAi-1
H
pGMR>bon; E(spl)mdelta-HLH
I
pGMR>bon; E(spl)m3-HLH
J
pGMR>bon
E(spl)m3-HLH
E(spl)mdelta-HLH
f-RNAi-2
f-RNAi-1
sha
w-RNAi-2
w-RNAi-1
GFP
Number of trichomes
K
pGMR>yki-S168A; GFP
L
pGMR>yki-S168A; sha
M
pGMR>yki-S168A; f-RNAi-1
N
pGMR>yki-S168A; E(spl)mdelta-HLH
O
pGMR>yki-S168A; E(spl)m3-HLH
P
pGMR>yki-S168A
Number of trichomes

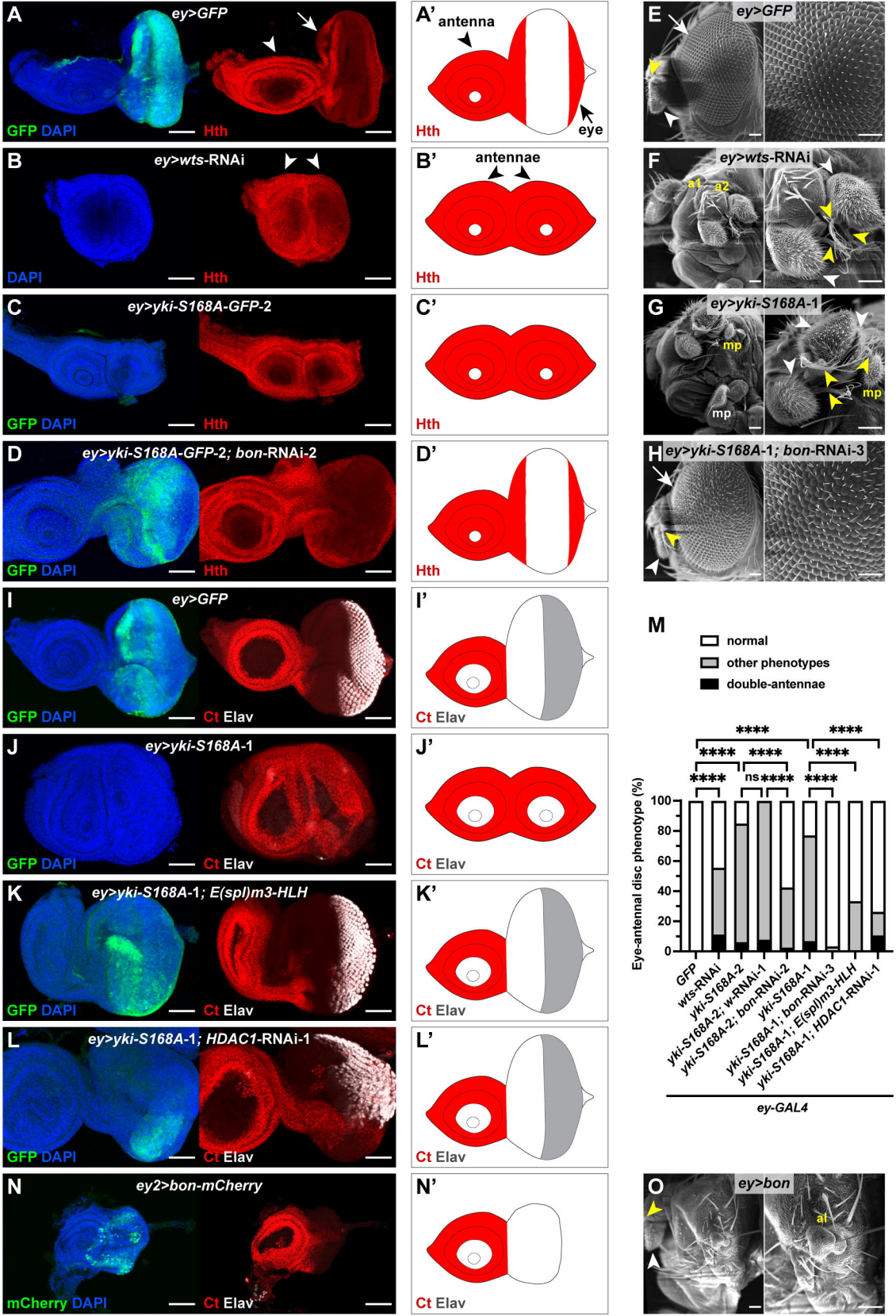
A
ey>GFP
GFP DAPI
Hth
A'
antenna
eye
Hth
B
ey>wts-RNAi
DAPI
Hth
B'
antennae
Hth
C
ey>yki-S168A-GFP-2
GFP DAPI
Hth
C'
Hth
D
ey>yki-S168A-GFP-2; bon-RNAi-2
GFP DAPI
Hth
D'
Hth
E
ey>GFP
F
ey>wts-RNAi
a1
a2
G
ey>yki-S168A-1
mp
mp
mp
H
ey>yki-S168A-1; bon-RNAi-3
I
ey>GFP
GFP DAPI
Ct Elav
I'
Ct Elav
J
ey>yki-S168A-1
GFP DAPI
Ct Elav
J'
Ct Elav
K
ey>yki-S168A-1; E(spl)m3-HLH
GFP DAPI
Ct Elav
K'
Ct Elav
L
ey>yki-S168A-1; HDAC1-RNAi-1
GFP DAPI
Ct Elav
L'
Ct Elav
N
ey2>bon-mCherry
mCherry DAPI
Ct Elav
N'
Ct Elav
M
normal
other phenotypes
double-antennae
Eye-antennal disc phenotype (%)
100
80
60
40
20
0
****
ns
GFP
wts-RNAi
yki-S168A-2
yki-S168A-2; w-RNAi-1
yki-S168A-2; bon-RNAi-2
yki-S168A-1
yki-S168A-1; bon-RNAi-3
yki-S168A-1; E(spl)m3-HLH
yki-S168A-1; HDAC1-RNAi-1
ey-GAL4
O
ey>bon
a1

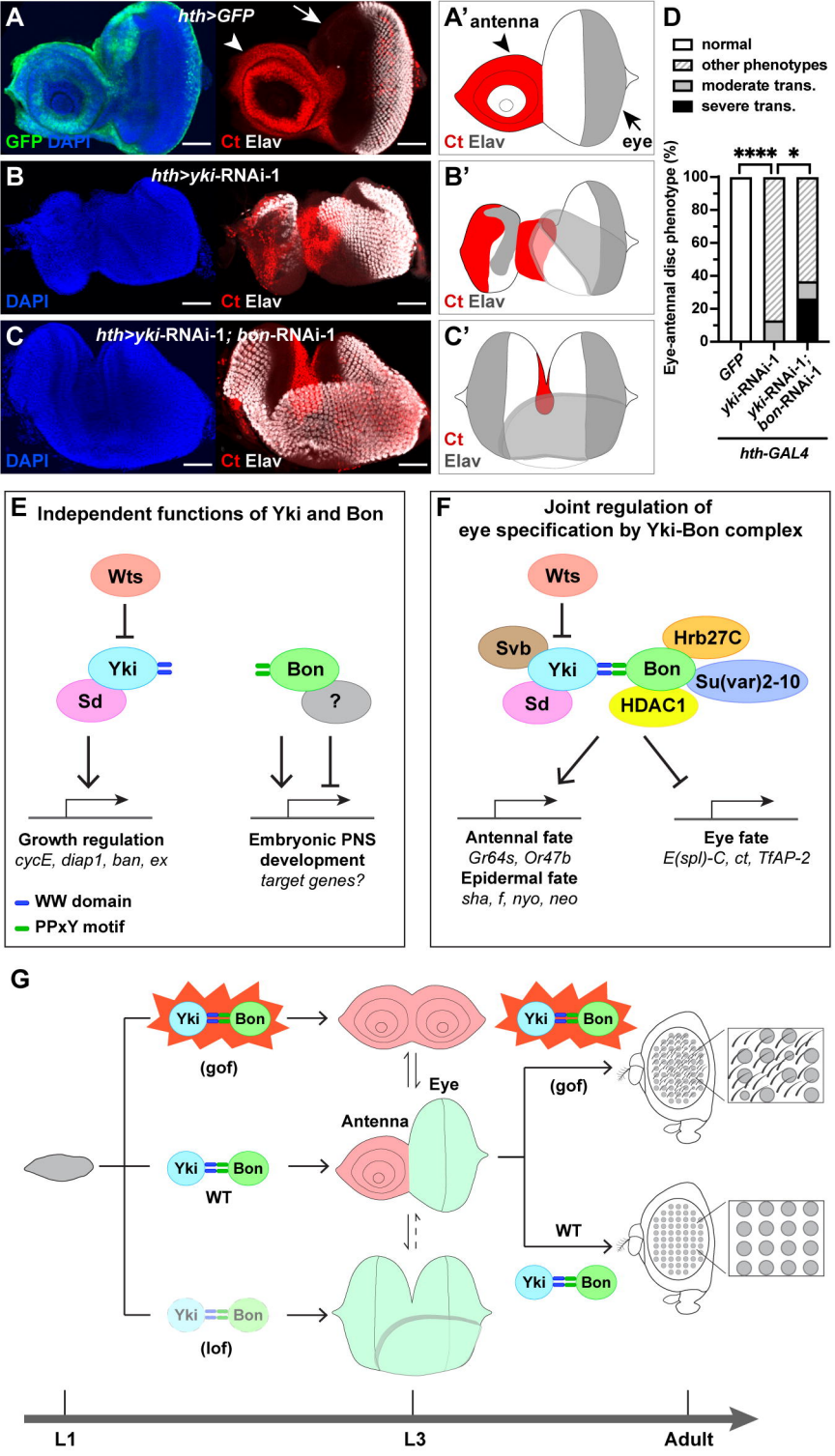
A
hth>GFP
GFP DAPI
Ct Elav
B
hth>yki-RNAi-1
DAPI
Ct Elav
C
hth>yki-RNAi-1; bon-RNAi-1
DAPI
Ct Elav
A' antenna
Ct Elav
eye
B'
Ct Elav
C'
Ct
Elav
D
normal
other phenotypes
moderate trans.
severe trans.
Eye-antennal disc phenotype (%)
100
80
60
40
20
0
****
*
GFP
yki-RNAi-1
yki-RNAi-1; bon-RNAi-1
hth-GAL4
E Independent functions of Yki and Bon
Wts
Yki
Sd
Bon
?
Growth regulation
cycE, diap1, ban, ex
Embryonic PNS development
target genes?
WW domain
PPxY motif
F Joint regulation of eye specification by Yki-Bon complex
Wts
Svb
Yki
Sd
Bon
Hrb27C
Su(var)2-10
HDAC1
Antennal fate
Gr64s, Or47b
Epidermal fate
sha, f, nyo, neo
Eye fate
E(spl)-C, ct, TfAP-2
G
Yki
Bon
(gof)
Eye
Antenna
WT
(lof)
L1
L3
Adult